GW8510 alleviates muscle atrophy and skeletal muscle dysfunction in mice through AMPK/PGC1α signaling

YUTONG CHEN[1-3], ZURUI LIU[4], CHEN LIU[4], DAQIAN YANG[1-3], MENGMENG XIAO[1], ZHENGQIAN LI[1] and ZHENGWEI XIE[1-5]

[1]Peking University International Cancer Institute, School of Basic Medical Sciences, Peking University Health Science Center, Beijing 100191, P.R. China; [2]Peking University-Yunnan Baiyao International Medical Research Center, Peking University Health Science Center, Beijing 100191, P.R. China; [3]State Key Laboratory of Natural and Biomimetic Drugs, Department of Molecular and Cellular Pharmacology, School of Pharmaceutical Sciences, Peking University Health Science Center, Beijing 100191, P.R. China; [4]Beijing Gigaceuticals Tech. Co. Ltd., Beijing 102206, P.R. China; [5]Beijing Life Science Academy, Beijing 102209, P.R. China

Received February 22, 2025; Accepted June 2, 2025

DOI: 10.3892/ijmm.2025.5569

Abstract. Preventing and restoring muscle loss and function is essential for elderly individuals. GW8510 may accelerate myotube differentiation. The present study aimed to investigate the protective effect of GW8510 (a CDK2 inhibitor) on muscle atrophy. Mouse models of muscle atrophy were induced by denervation, dexamethasone and glycerol. Muscle-to-body weight ratio, the cross-sectional area of muscles, grip strength, fatigue and serum levels of superoxide dismutase and creatine kinase were assessed. *In vitro*, a dexamethasone-induced C2C12 myotube atrophy model was used to evaluate mitochondrial function. Reverse transcription-quantitative PCR, immunoblotting and small interfering RNA transfection were performed to explore the potential molecular mechanisms following treatment with GW8510. GW8510 resulted in a significant increase in the gastrocnemius and soleus muscle ratios in denervation mice (7 and 3%, respectively), alongside an increase in cross-sectional area. Moreover, GW8510 significantly improved grip strength and superoxide dismutase activity, with similar protective effects in dexamethasone- and glycerol-induced muscle atrophy models. GW8510 decreased reactive oxygen species production, increased mitochondrial DNA copy number, maintained mitochondrial dynamics and enhanced antioxidant activity in C2C12 myotubes. Mechanistically, GW8510 significantly inhibited the expression of atrophy-associated markers F-box protein 32 and tripartite motif-containing 63 while activating AMPK (both $P<0.01$). The knockdown peroxisome proliferator-activated receptor-γ co-activator-1α (Pgc1α) negated the effects of GW8510. Overall, GW8510 mitigated muscle atrophy via the activation of the AMPK/PGC1α pathway. GW8510 could serve as a novel therapeutic agent for the prevention of muscle atrophy.

Introduction

Sarcopenia is an aging-associated disease characterized by losing skeletal muscle mass and function (1). Disrupted proteostasis, which leads to increased protein degradation via the ubiquitin-proteasome system, triggers muscle atrophy (2,3). Two muscle-specific ubiquitin ligases, F-box protein 32 (Fbxo32) and tripartite motif containing 63 (Trim63), serve roles in the progression of muscle atrophy (4). Inhibiting Fbxo32 suppresses the expression of myostatin (Mstn), a negative regulator of muscle that protects against atrophy in fasting mice (5). Additionally, Trim63 knockout mice maintain protein synthesis and prevent muscle atrophy induced by dexamethasone (6).

Mitochondrial dysfunction contributes to muscle atrophy through mechanisms such as mitophagy (7), mitochondrial fission-fusion (8) and mitochondrial biogenesis (9). Resistance and endurance training are employed to improve muscle atrophy and frailty in older adults (10). The search for pharmacological interventions to maintain and improve muscle mass and function is key for healthy aging.

GW8510 is a cyclin-dependent kinase 2 (CDK2) inhibitor that can increase insulin expression by activating p53 transcriptional activity (11). Protein expression of CDK2 is reduced during myogenesis, and CDK2 activates RB transcriptional corepressor 1 and disrupts myogenic differentiation 1 (Myod1)

Correspondence to: Professor Zhengwei Xie, Peking University International Cancer Institute, School of Basic Medical Sciences, Peking University Health Science Center, 38 Xueyuan Road, Haidian, Beijing 100191, P.R. China
E-mail: xiezhengwei@hsc.pku.edu.cn

Abbreviations: Mstn, myostatin; CDK2, cyclin-dependent kinase 2; CMC-Na, sodium carboxymethyl cellulose; GC, gastrocnemius; SOL, soleus; TA, tibialis anterior; EDL, extensor digitorum longus; Quad, quadriceps; SOD, superoxide dismutase; CK, creatine kinase; ROS, reactive oxygen species; mtDNA, mitochondrial DNA; GSH, glutathione; MDA, malondialdehyde; CSA, cross-sectional area; OXPHOS, oxidative phosphorylation; AMPK, AMP-activated protein kinase

Key words: GW8510, denervation, dexamethasone, muscle atrophy, AMPK, Pgc1α

function to inhibit myogenesis (12). Additionally, GW8510 accelerates myotube differentiation via activation of transcription of Myod1 in human myogenic cell line LHCN-M2 (13), which indicates that CDK2 may serve an essential role in skeletal muscle differentiation. Furthermore, GW8510 induces autophagy and apoptosis to suppress the progression of numerous types of cancer, such as pancreatic (14), breast (15) and colorectal cancer (16), lung squamous cell carcinoma (17) and non-small cell lung cancer (18). In addition, GW8510 suppresses the death of cerebellar granule neurons to prevent neuronal apoptosis and exerts a protective effect in Parkinson's disease (19,20). These findings also indicate that GW8510 may ameliorate and prevent the development and progression of aging-related diseases. However, the pharmacological effects of GW8510 on muscle atrophy treatment remain unclear. The present study aimed to explore whether GW8510 alleviates muscle loss and function in various mouse models of muscle atrophy and demonstrate the potential underlying mechanisms.

Materials and methods

Animal experiments. All animal experiments were approved by and performed in strict accordance with the guidelines of the Ethics Committee of Peking University Health Science Centers (approval no. DLASBD0122; Beijing, China). Male ICR mice (age, 6 weeks; weight, 20-22 g, n=48) were purchased from the Department of Laboratory Animal Science of Peking University Health Science Center. All mice were raised with free access to food and water under a 12/12-h light/dark cycle and humidity (55±5%) at 22±2˚C.

Sciatic denervation-induced muscle atrophy model. Sham mice (n=5) at the age of 8 weeks were administered intraperitoneal 0.5% sodium carboxymethyl cellulose (CMC-Na) for 21 consecutive days, followed by exposure of sciatic nerve. Vehicle mice (n=6) were administered intraperitoneal 0.5% CMC-Na for 21 consecutive days, followed by the dissection of the sciatic nerve after anesthesia. GW8510 mice (n=6) were administered intraperitoneal GW8510 (purity, 99.5%, WuXi AppTec) dissolved in 0.5% CMC-Na for 14 consecutive days, followed by sciatic nerve dissection. GW8510 was then administered for a further 7 days. The muscle strength was assessed by grip strength test following sciatic denervation. Mice were sacrificed 7 days post-sciatic denervation, with no loss of mobility or severe behavioral abnormality observed before the endpoint (21).

Dexamethasone-induced muscle atrophy model. Sham mice (n=5) at the age of 8 weeks were administered intraperitoneal 5 DMSO + 5 Tween-80 + 90% saline for 14 consecutive days (22). Vehicle mice (n=6) were administered intraperitoneal dexamethasone (10 mg/kg) and 0.5% CMC-Na for 14 consecutive days. GW8510 mice (n=6) were simultaneously administered intraperitoneal dexamethasone (10 mg/kg) and GW8510 (2 mg/kg) for 14 days. The muscle strength was assessed by grip strength test on day 7 of dexamethasone injection. Mice were sacrificed 14 days following final dexamethasone injection, with no loss of mobility or severe behavioral abnormality observed before the endpoint.

Glycerol-induced muscle injury model. Sham mice (n=4) at the age of 8 weeks were administered intraperitoneal 0.5% CMC-Na for 14 consecutive days, followed by the intramuscular injection of 0.9% saline into the gastrocnemius (GC) muscle. Vehicle mice (n=5) were administered intraperitoneal 0.5% CMC-Na for 14 consecutive days, followed by the intramuscular injection of glycerol (100 μl, 50% v/v) into the GC. GW8510 mice (n=5) were administered intraperitoneal GW8510 (2 mg/kg) for 14 consecutive days, followed by the intramuscular injection of glycerol (100 μl, 50% v/v) into the GC. The muscle strength was assessed by grip strength test on day 3 day of glycerol injection. Mice were subjected to intramuscular injection of glycerol at day 9 and sacrificed 5 days flater, with no loss of mobility or severe behavioral abnormality observed before the endpoint (23).

Mice were euthanized by cervical dislocation and the GC, soleus (SOL), tibialis anterior (TA), extensor digitorum longus (EDL) and quadriceps (Quad) muscles were collected and weighed. The muscle to body weight ratio was measured to assess the degree of muscle atrophy. All muscle tissues were stored at 80˚C for further analysis.

Histology. The GC and SOL in denervation and dexamethasone-induced and GC and TA in glycerol-induced muscle atrophy mice were fixed in 4% paraformaldehyde solution for 48 h at room temperature. Paraffin-embedded sections (5 μm) were stained with hematoxylin and eosin for 5 min at room temperature. Stained slides were viewed using a light microscope, scanned by Panoramic SCAN II (3DHISTECH) and images were captured by CaseViewer software (version 2.9.0, 3dhistech.com/news/caseviewer-becomes-slideviewer/). The cross-sectional area (CSA) was measured using ImageJ (version 1.54; National Institutes of Health).

Behavioral test. The muscle fatigue test was performed using the rotarod apparatus (23,24). Briefly, mice were pre-trained on an accelerating rotarod for 10 min once/day for 3 days. In the formal test, mice were placed on the rotarod apparatus with speeds ranging from 5 to 40 rpm. The latency to fall off the rotarod was recorded. The grip strength test was performed using a grip strength device (Yiyan Technology Co., Ltd.) and the maximal force of all four limbs was recorded. The grip strength test of mice was repeated five times, and the mean grip strength was analyzed.

Cell culture, differentiation and treatment. Mouse C2C12 myoblasts were purchased from Procell Life Science & Technology Co., Ltd. and authenticated by STR profiling. Cells were cultured in DMEM (Macgene; cat. no. CM10013) supplemented with 10% FBS (Yeasen; cat. no. 40130ES76) and 1% penicillin-streptomycin with 5% CO_2 at 37˚C. To induce differentiation, cells were seeded into 6-well plates starting at density of $4x10^5$ cells each well and maintained with differentiation medium (DMEM containing 2% horse serum (Beijing Solarbio Science & Technology Co., Ltd.; cat. no. S9050) and the differentiation medium was replaced every 48 h for 6 days at 37˚C. To induce muscle atrophy *in vitro*, C2C12 cells were stimulated with 10 μM dexamethasone (TargetMol Chemicals Inc.; cat. no. T1076) or 20 ng/ml TNFα (Novoprotein Scientific Inc.; cat. no. CF09) for 24 h at 37˚C. Then, C2C12 cells were treated with DMSO or GW8510 (2 μM, dissolved in 0.1% DMSO) for another 24 h at 37˚C.

Cell Counting Kit-8 (CCK-8) assay. Viability of C2C12 myoblasts after GW8510 treatment was performed using CCK-8 (Shanghai Yeasen Biotechnology Co., Ltd.; cat. no. 40203ES60). Briefly, C2C12 myoblasts were seeded in a 96-well plate at density of $5x10^3$ cells each well and treated with GW8510 (0.25, 0.50, 1.00, 2.00, 4.00 and 8.00 μM) for 24 h at 37˚C. A total of 10 μl/well CCK-8 solution was added for 2 h. The absorbance was captured by a Synergy H1 microplate reader (BioTek; Agilent Technologies, Inc.), with a wavelength of 450 nm.

Morphological analysis of C2C12 myotubes. C2C12 myotubes were stained using Hematoxylin and Eosin Staining kit (Beyotime Institute of Biotechnology; cat. no. C0105S) according to the manufacturer's instructions. Briefly, C2C12 cells were fixed in 4% paraformaldehyde solution for 20 min at room temperature and washed with distilled water twice. C2C12 myotubes were stained with hematoxylin for 5 min at room temperature, washed with tap water, stained with eosin for 2 min and washed with 70% ethanol. Images were captured in five randomly selected fields of view using a light microscope. The myotube length and diameter were measured using ImageJ (version 1.54; National Institutes of Health).

Reverse transcription-quantitative (RT-q)PCR. In brief, total RNA in C2C12 myotubes was extracted using Rapure Total RNA kit (Magen Biotechnology Co., Ltd.; cat. no. R4011-03). Then, cDNA was reverse-transcribed by StarScript III All-in-one RT Mix according to the manufacturer's instructions. (cat. no. A230-100; Beijing Kangrun Chengye Biotechnology Co., Ltd.). Finally, qPCR was performed using 2XRealStar Fast SYBR qPCR Mix (Beijing Kangrun Chengye Biotechnology Co., Ltd.; cat. no. A304-10). The thermal cycling protocol was under the following conditions: initial cycle at 95˚C for 120 sec, followed by 40 cycles of denaturation at 95˚C for 15 sec, combined annealing/extension at 60˚C for 30 sec. TATA-box binding protein expression was used as internal control and target gene expression was quantified by the relative quantification (2-ΔΔCq) method (25). The primers are listed in Table I.

Superoxide dismutase (SOD) and creatine kinase (CK) activity. The activity of SOD and CK in serum of muscle atrophy mice and in C2C12 cells was measured using a SOD (cat. no. A001-3-2) and CK assay kit (both Nanjing Jiancheng Bioengineering Institute; cat. no. A032-1-1) according to the manufacturer's instructions.

Reactive oxygen species (ROS) measurement. The production of ROS was assessed using the ROS Assay kit (Beyotime Institute of Biotechnology; cat. no. S0033S) according to the manufacturer's instructions. Briefly, C2C12 myotubes were incubated with 10 μM DCFH-DA for 30 min at 37˚C and washed with PBS three times. Images were captured of five randomly selected fields of view using a fluorescence microscope.

Mitochondrial mass measurement. Mitochondrial mass was measured using Mito-Tracker Deep Red FM staining (Beyotime Institute of Biotechnology; cat. no. C1032) according to the manufacturer's instructions. Briefly, C2C12 myotubes were incubated with 10 nM Mito-Tracker Deep Red FM at 37˚C and washed with PBS three times. The fluorescence intensity was captured by Synergy H1 microplate reader (BioTek; Agilent Technologies, Inc.), with the excitation wavelength of 644 nm and emission wavelength of 665 nm.

Mitochondrial DNA (mtDNA) copy number analysis. Genomic DNA in C2C12 was isolated using the Universal Genomic DNA Purification Mini Spin kit (Beyotime Institute of Biotechnology; cat. no. D0063) according to the manufacturer's instructions. Thermocycling conditions were as follows: Initial cycle at 95˚C for 120 sec, followed by 40 cycles of denaturation at 95˚C for 15 sec, combined annealing/extension at 60˚C for 30 sec. and Gapdh expression was used as a nuclear DNA control. The primer of mtDNA was as follows: Forward, 5'-ACCGCAAGGGAAAGATGAAAG-3' and reverse, 5'-AGG TAGCTCGTTTGGTTGGTTTCGG-3'.

NAD^+/NADH ratio and ATP measurement. NAD^+ and ATP levels in GC of denervation-induced muscle atrophy mice and C2C12 myotubes was measured using NAD^+/NADH Assay kit with WST-8 (cat. no. S0175) and ATP Assay kit (both Beyotime Institute of Biotechnology; cat. no. S0026) according to the manufacturer's instructions, to evaluate the function of mitochondria following treatment with GW8510.

Glutathione (GSH) and malondialdehyde (MDA) content measurement. The content of reduced GSH in serum and GC tissue of denervation-induced muscle atrophy mice and MDA in GC of denervation-induced muscle atrophy mice and C2C12 myotubes was measured using Cell MDA (cat. no. A003-4-1) and Reduced GSH assay kits (both Nanjing Jiancheng Bioengineering Institute; cat. no. A006-2-1) according to the manufacturer's instructions, to evaluate antioxidation ability following treatment with GW8510.

RNA-sequencing (seq) analysis. Total RNA in C2C12 myotubes was isolated and purified using TRIzol (Invitrogen; Thermo Fisher Scientific, Inc.) following the manufacturer's procedure. The RNA and purity of each sample was quantified using NanoDrop ND-1,000 (NanoDrop). The RNA integrity was assessed by Bioanalyzer 2100 (Agilent) with RIN number >7.0, and confirmed by electrophoresis with denaturing agarose gel. A total of 1 μg RNA was applied for library construction. Then, 2x150 bp paired-end sequencing was performed using Illumina NovaSeq 6000 S4 Reagent kit v1.5 (300 cycles; cat. 20028312; Illumina Inc.) on Illumina Novaseq™ 6000 (Hangzhou Lianchuan Biotechnology Co., Ltd.) following the manufacturer's protocol. Fastp software (github.com/OpenGene/fastp, version: fastp-0.26.0) was used to remove the reads that contained adaptor contamination, low-quality bases and undetermined bases with default parameters. HISAT2 (https://ccb.jhu.edu/software/hisat2, version: hisat2-2.2.1) was used to map reads to the reference genome of *Mus musculus* GRCm39 GENCODE vM30. StringTie (http://ccb.jhu.edu/software/stringtie/, version: stringtie-2.1.6) was used to determine expression of mRNAs by calculating Fragments Per Kilobase of exon model per Million mapped fragments (FPKM) as follows:

$$FPKM = \frac{total\_exon\_fragments}{mapped\_reads(millions)} \times exon\_length(kB)$$

Table I. Primers for reverse transcription-quantitative PCR.

Gene	Forward, 5'→3'	Reverse, 5'→3'
Myog	CTTGCTCAGCTCCCTCAACC	GCCGCGAGCAAATGATCTCC
Fbxo32	TGAGCGACCTCAGCAGTTAC	GCGCTCCTTCGTACTTCCTT
Trim63	ACCACAGAGGGTAAAGAAGAACA	TGGGGAGCCCTATGCTAGTC
Mstn	ATTGGCTCAAACAGCCTGAA	TTCTAAAAAGGGATTCAGCCCA
Fam132b	TTATCCCATCTGAGGTTCTG	CAGATGGCTCTCTCGCT
Acta2	TTTCATTGGGATGGAGTCAG	TCCTTCCTGATGTCAATATCAC
Tgfb1	ACCAAGGAGACGGAATACAG	CGTTGATTTCCACGTGGAG
Pgc1α	CCCTGCCATTGTTAAGACC	TGCTGCTGTTCCTGTTTTC
Tfam	CCAAGTCAGCTGATGGGTATGG	CCTGAGCCGAATCATCCTTTGC
Sirt1	TCCTCACTAATGGCTTTCATTCCTG	GTGCCAATCATGAGATGTTGCTG
Nrf1	GAGCACGGAGTGACCCAAAC	TGTACGTGGCTACATGGACCT
Sod1	CATGGCGATGAAAGCGGTGT	CTGCACTGGTACAGCCTTGTG
Sod2	CCACACATTAACGCGCAGAT	AGGGCTCAGGTTTGTCCAGA
Cat	CTGGAGTCTTCGTCCCGAGT	CTTCCTGCCTCTCCAACAGG
Myf5	TCTGACGGCATGCCTGAAT	AAGCTGGACACGGAGCTTTT
Myf6	AGTGGCCAAGTGTTTCGGAT	ATCCACGTTTGCTCCTCCTTC
Myof	GGGGAGAAGTGGAAGCAACT	GCTATACTTCCGCCTTCGCT
Gadd45a	AGAGCAGAAGACCGAAAGGATG	GCACGGATGAGGGTGAAATG
Ncam1	CACAGCCAGTCCGGGAAC	AGGGACTTGAGCATGACGTG
Chrna1	CCAGGAGTCCAATAACGCCG	CAATGAGCCGACCTGCAAAC
Pink1	GTGGACCATCTGGTTCAGCA	CAGGGACAGCCATCTGAGTC
Sqstm1	GGACCCATCTACAGAGGCTG	ATCACAATGGTGGAGGGTGC
Map1lc3b	GAGGGGACCCTAACCCCATA	TCGCTCTATAATCACCCGCC
Atg12	TAAACTGGTGGCCTCGGAAC	CCATCACTGCCAAAACACTCA
Atg5	TCTTGGTGACGTCATCTCCG	CAACCAAAGCCAAACCGAGG
Cdk2	CGGAGTGGTGTACAAAGCCA	ACACCTTCAGTCTCAGTGTCG
p21	CAGAATAAAAGGTGCCACAGGC	CGTCTCCGTGACGAAGTCAA
p16	TGAATCTCCGCGAGGAAAGC	TGCCCATCATCATCACCTGAA
Bnip3	TTCTCACTGTGACAGCCCAC	TCTTCCTCAGACAGAGTGCT
Tbp	ACCCTTCACCAATGACTCCTATG	TGACTGCAGCAAATCGCTTGG
Gapdh	ACCCTTAAGAGGGATGCTGC	CCCAATACGGCCAAATCCGT

Myog, myogenin; Fbxo32, F-box protein 32; Trim63, tripartite motif-containing 63; Mstn, myostatin; Fam132b, erythroferrone; Acta2, actin α2, smooth muscle, aorta; Tgfb1, transforming growth factor beta 1; Pgc, peroxisome proliferator-activated receptor gamma, coactivator; Tfam, transcription factor A, mitochondrial; Sirt, sirtuin; Sod, superoxide dismutase; Cat, catalase; Myf, myogenic factor; Myof, myoferlin; Gadd45a, growth arrest and DNA damage inducible alpha; Ncam1, neural cell adhesion molecule 1; Chrna, cholinergic receptor nicotinic alpha; Pink, PTEN induced kinase; Sqstm, sequestosome; Map1lc3b, microtubule associated protein 1 light chain 3 beta; Atg, autophagy related; Cdk, cyclin dependent kinase; Bnip, BCL2 interacting protein; Tbp, TATA-box binding protein.

Principal component analysis and differential gene expression analysis was performed using the edgeR (https://bioconductor.org/packages/release/bioc/html/edgeR.html; version 4.6.2) package. Genes with the false discovery rate <0.05 and absolute fold-change ≥2 were considered differentially expressed genes (DEGs). Gene Ontology (GO; http://www.geneontology.org/) and Kyoto Encyclopedia of Genes and Genomes pathway (KEGG; https://www.kegg.jp/) enrichment analysis was performed using the Database for Annotation, Visualization and Integrated Discovery (https://david.ncifcrf.gov/) for DEGs.

Transfection of small interfering (si)RNA. siRNAs targeting peroxisome proliferator-activated receptor-γ co-activator-1α (Pgc1α), negative or positive control (sequence-1, forward, 5'-CCGCAAUUCUCCCUUGUAUTT-3' and reverse, 5'-AUACAAGGGAGAAUUGCGGTT-3'; sequence-2, forward, 5'-CCCACAGGAUCAGAACAAATT-3' and reverse, 5'-UUUGUUCUGAUCCUGUGGGTT-3'; sequence-3', forward, 5'-GCCAAACCAACAACUUUAUTT-3' and reverse, 5'-AUAAAGUUGUUGGUUUGGCTT-3'; negative control, forward, 5'-UUCUCCGAACGUGUCACGUTT-3' and reverse, 5'-ACGUGACACGUUCGGAGAATT-3'; positive control, forward, 5'-AGAAUCCGAAGCUUGUCAUCAATT-3' and reverse, 5'-UUGAUGACAAGCUUCCCAUUCUTT-3', Haixing Biosciences Co., Ltd.; 100 nM) were mixed with Lipofectamine 3000 (Thermo Fisher Scientific, Inc.) for

20 min at room temperature in Opti-MEM® (Thermo Fisher Scientific, Inc.) and transfected into C2C12 myoblasts (~70% confluence) in a 6-well plate. Following transfection for 6 h at 37˚C, the medium was refreshed. Then, cells were differentiated for 4 days and transfected with siRNA every 48 h. Finally, C2C12 cells were treated with 2 μM GW8510 for 24 h at 37˚C and harvested for further experiments.

Western blot (WB) analysis. In brief, GC tissue and C2C12 myotubes were homogenized with cold RIPA (Beyotime Institute of Biotechnology) containing 1% protease and phosphatase inhibitor and the protein concentration was determined by BCA assay. A total of 10 μg/lane protein was separated by 10% SDS-PAGE and transferred to a nitrocellulose (NC) membrane. The NC membrane was blocked by 10% defatted milk at room temperature for 2 h and incubated at 4˚C overnight with the following primary antibodies: Anti-Cdk2 (; cat. no. AF1063; Beyotime Institute of Biotechnology.), anti-p21 (cat. no. YP-mAb-16762; Hangzhou Zhenyoupin Biotechnology Co., Ltd.), anti-p16 (1:1,000: cat. no. YP-mAb-16759; Hangzhou Zhenyoupin Biotechnology Co., Ltd.), anti-myogenin (Myog, 1:1,000; cat. no. sc-52903; Santa Cruz Biotechnology, Inc.), anti-Fbxo32 (1:1,000; cat. no. ab168372; Abcam), anti-tripartite motif-containing 63 (Trim63; cat. no. A3101; ABclonal Biotech Co., Ltd.), anti-mitofusin 1 (Mfn1; all 1:1,000; cat. no. ab126575; Abcam), anti-OPA1 mitochondrial dynamin-like GTPase (OPA1, 1:1,000; cat. no. ab119685; Abcam), anti-phosphorylated (p-) Dynamin related protein 1 (Drp1, 1:1,000; cat. no. 4494; Cell Signaling Technology, Inc.), anti-Drp1 (1:1,000; cat. no. 12957; Proteintech Group, Inc.), anti-AMPK (cat. no. AF6195; Beyotime Institute of Biotechnology), anti-p-AMPK (; cat. no. AA393), anti-MSTN (all 1:1,000; cat. no. AF7512; all Beyotime Institute of Biotechnology), anti-PGC1α (1:1,000.; cat. no. 66369; Proteintech Group, Inc.), anti-Erk1/2 (1:1,000; cat. no. 9102; Cell Signaling Technology, Inc.), anti-p-Erk1/2 (1:1,000; cat. no. 4370; Cell Signaling Technology, Inc.), anti-oxidative phosphorylation (OxPhos) Rodent WB Antibody Cocktail (1:500; cat. no. 45-8099; Invitrogen; Thermo Fisher Scientific, Inc.), anti-β-actin (1:5,000: cat. BE0037; EASYBIO), anti-GAPDH (1:5,000: cat. BE0023) and anti-β-tubulin (1:5,000: cat. BE0025; all EASYBIO). The membrane was washed three times with Tris-buffered saline containing 0.1% Tween-20 and then incubated with corresponding horseradish peroxidase-conjugated secondary antibodies (1:5,000) at room temperature for 1 h. Then, bands were detected by Super ECL Detection Reagent (Shanghai Yeasen Biotechnology Co., Ltd.). The images were analyzed by ImageJ software (version 1.54; National Institutes of Health).

Statistical analysis. All data are presented as the mean ± SEM from three independent experiments. Continuous variables between groups were compared using one- or two-way ANOVA followed by Tukey's post hoc test. All statistical analyses were performed in GraphPad Prism (version 9.0.0; Dotmatics). $P<0.05$ was considered to indicate a statistically significant difference.

Results

GW8510 improves muscle atrophy and weakness in mice with denervation of the sciatic nerve. To investigate the effect of GW8510 on muscle mass, a mouse model of muscle atrophy was established by dissection of the sciatic nerve and treatment with GW8510. There was no significant difference in body weight between the sham, the denervated and the mice treated with GW8510. The ratio of muscle to body weight in GC and SOL tissues reduced significantly by 30 and 26% in denervation compared with sham group, respectively, whereas treatment with GW8510 2 mg/kg increased this ratio by 7 and 3%. Moreover, the ratios for TA, EDL, and Quad tissue exhibited no significant difference in the mice treated with GW8510 (Fig. 1). Furthermore, the mean CSA was smaller in GC and SOL tissue in the denervated mice with muscle atrophy; this decrease was ameliorated by GW8510 (Fig. 2A). The mean CSA was smaller and the frequency distribution of CSA in GC and SOL decreased in the group with denervated mice but increased by GW8510 (Fig. 2B).

The effect of GW8510 on muscle function was evaluated using the grip strength and muscle fatigue tests. Tests using the accelerating rotarod system showed that grip strength was weaker and latency to fall off was shorter in denervated than in the sham mice (Fig. 2C). GW8510 improved grip strength significantly, but not latency to fall off (Fig. 2C). The activity of SOD was lower in the denervated than in the sham mice but was increased by GW8510 (Fig. 2D). However, the activity of CK was lower in the denervated mice and had no significant difference in mice treated with GW8510 (Fig. 2D). In summary, GW8510 improved muscle atrophy and weakness in mice with denervation of the sciatic nerve.

GW8510 prevents muscle atrophy induced by dexamethasone. The effect of GW8510 was examined in ICR mice with muscle atrophy established by intraperitoneal injection of dexamethasone. Body weight was significantly decreased in mice with dexamethasone-induced muscle atrophy in comparison with the sham mice and was not changed by treatment with GW8510 (Fig. S1). The ratio of muscle to body weight was reduced but improved by treatment with GW8510 in TA and SOL tissues but not in GC, EDL or Quad tissues (Fig. S1). The mean CSA was smaller and the frequency distribution of CSA in GC and TA tissue was reduced in the group with dexamethasone-induced muscle atrophy but increased by GW8510 (Fig. S2A and B). Furthermore, grip strength was weaker in the mice with dexamethasone-induced muscle atrophy than in the sham mice and was improved significantly by GW8510 (Fig. S2C); however, GW8510 had no significant effect on latency to fall off, which was consistent with the findings in the denervated mice (Fig. S2C). Serum CK activity was higher in mice with dexamethasone-induced muscle injury than in the sham mice, indicating worse muscle atrophy, which was restored to normal by GW8510 (Fig. S2D). However, there was no change in SOD activity in response to GW8510 (Fig. S2D).

GW8510 prevents muscle injury induced by glycerol. Similarly, the effect of GW8510 was examined in ICR mice with muscle injury established by intramuscular injection of glycerol into GC tissue. There was no significant difference in body weight between the sham, the mice with glycerol-induced muscle injury and mice treated with GW8510. The ratio of muscle to body weight was lower in GC and Quad tissue in the mice with glycerol-induced muscle injury compared with the sham group

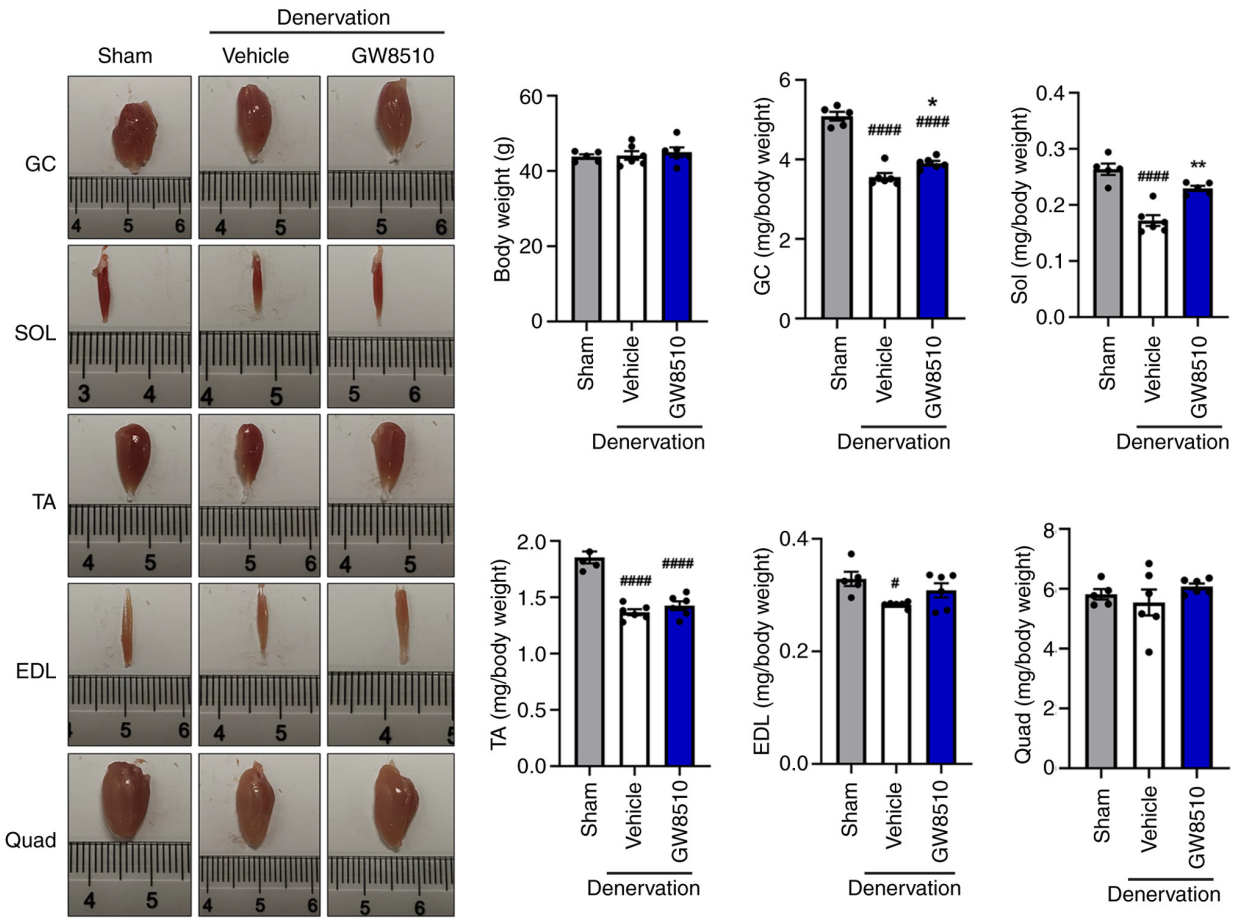

Figure 1. GW8510 improves muscle atrophy and weakness in sciatic nerve denervation mice. Mouse body weight and muscle/body weight ratio of skeletal muscle. n=5-6/group. $^{\#}$P<0.05, $^{\#\#\#\#}$P<0.0001 vs. sham; *P<0.05, **P<0.01 vs. vehicle. GC, gastrocnemius; SOL, soleus; TA, tibialis anterior; EDL, extensor digitorum longus; Quad, quadriceps.

and improved by GW8510 (Fig. S3). By contrast, GW8510 had no effect on SOL, TA and EDL tissue. The mean CSA was smaller and the frequency distribution of CSA in GC and SOL tissue was lower in the mice with glycerol-induced muscle injury compared with those in sham group and had no significant difference in mice treated with GW8510 (Fig. S4A and B). GW8510 significantly improved grip strength but not the latency to fall off in the mice with glycerol-induced muscle injury (Fig. S4C). Serum SOD activity was lower in the mice with glycerol-induced muscle injury than in the sham mice, indicating more severe muscle injury, and was improved by GW8510 (Fig. S4D). However, GW8510 had no significant effect on CK activity (Fig. S4D). Overall, GW8510 prevented muscle atrophy and injury in the mouse model of muscle damage induced by glycerol.

GW8510 ameliorates dexamethasone-induced atrophy of myotubes in C2C12 myoblasts. To determine the safe dose of GW8510, viability of C2C12 myoblasts treated with GW8510 was assessed. Results showed that 0.25, 0.50, 1.00 and 2.00 μM exerted no significant toxicity (Fig. 3A). mRNA and protein expression of the atrophy-related genes Fbxo32 and Trim63 was assessed. GW8510 reduced the mRNA and protein expression of Fbxo32 and Trim63, and 2 μM GW8510 had the most significant effect (Fig. 3A and B). Therefore, 2 μM GW8510 was selected for further experiments.

To explore the effect of GW8510 as a CDK2 inhibitor *in vitro*, C2C12 mouse myoblasts were differentiated into myotubes for examination of the expression of cell cycle-related genes (p21 and p16). GW8510 significantly increased mRNA expression of p21 and reduced the mRNA and protein expression of p16 (Fig. S5A and B) but had no significant effect on the p21 protein level compared with dexamethasone group (Fig. S5B).

C2C12 myoblasts were stimulated with 10 μM dexamethasone and then treated them with 2 μM GW8510. Length and diameter of the myotubes decreased following stimulation with dexamethasone, indicating damage *in vitro*, which was ameliorated by GW8510 (Fig. 3D). The diameter of the myotubes decreased significantly by 48% in dexamethasone compared with control group, but increased by 39% after treatment with 2 μM GW8510 (Fig. 3D). Furthermore, dexamethasone-induced elevation of expression of the atrophy-associated genes Fbxo32 and Trim63 in dexamethasone group was reversed by GW8510 (Fig. 3E). In the present study, the expression of Myog did not change in response to stimulation by dexamethasone but decreased following treatment with GW8510. Furthermore, the dexamethasone-induced increases in protein expression of Myog, Fbxo32 and Trim63 were reversed by GW8510 (Fig. 3F). GW8510 significantly increased the activity of SOD and decreased that of CK in C2C12 cells (Fig. 3G). As excessive fibrosis negatively impacts

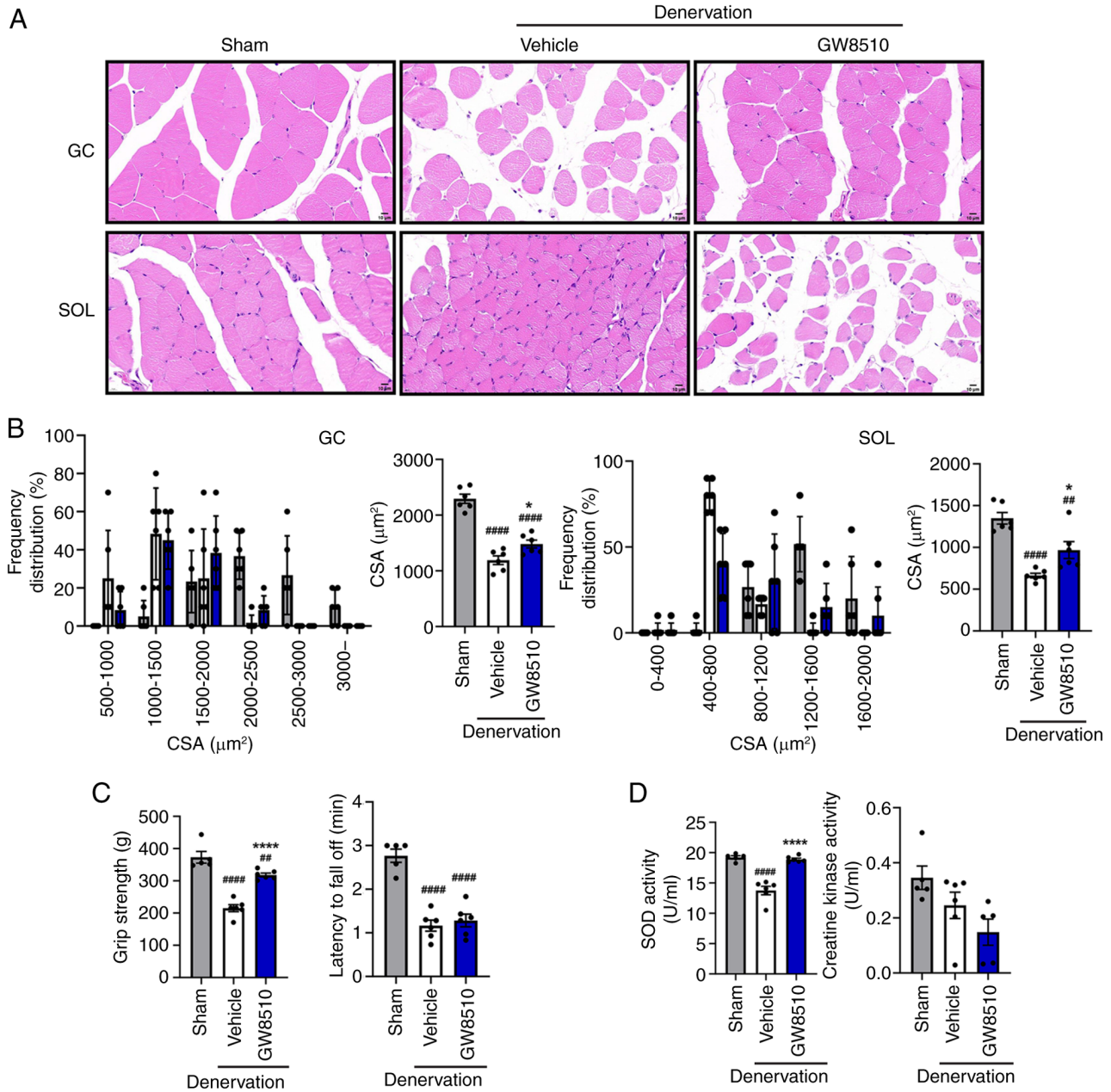

Figure 2. GW8510 improves muscle atrophy in GC and SOL in denervation mice. (A) Hematoxylin and eosin staining. Scale bar, 10 μm. (B) Mean CSA distribution of GC muscle. n=6/group. (C) Maximal grip strength in four limbs and latency to fall off on day 4 after dissection of the sciatic nerve. (D) Activity of SOD and creatine kinase. n=5-6/group. $^{\#\#}$P<0.01, $^{\#\#\#\#}$P<0.0001 vs. sham; *P<0.05, ****P<0.0001 vs. vehicle. GC, gastrocnemius; SOL, soleus; CSA, cross-sectional area; SOD, superoxide dismutase.

muscle function and regeneration of muscle fibers (26), expression of the fibrosis-related genes Acta2 and Tgfb1 was assessed; GW8510 significantly reduced their mRNA expression levels (Fig. 3H). These findings indicated that GW8510 ameliorated dexamethasone-induced atrophy of C2C2 myotubes *in vitro*.

GW8510 improves mitochondrial function and biogenesis in C2C12 myotubes. Mitochondrial dysfunction contributes to atrophy of skeletal muscle, and denervation reduces the mitochondrial biomass and impairs mitochondrial function (27,28). Therefore, the effect of GW8510 on the functional status of the mitochondria was assessed. C2C12 myotubes were stained with DCFH-DA to measure production of ROS under a fluorescence microscope; dexamethasone-induced increase in fluorescence intensity was decreased by GW8510 (Fig. 4A and B). C2C12 myotubes were stained with Mitotracker DeepRed to evaluate the mitochondrial mass, which detected an increase in relative fluorescence intensity following treatment with GW8510, indicating that GW8510 increased the mitochondrial mass in dexamethasone-induced C2C12 myotubes (Fig. 4C). mtDNA copy number increased following treatment with GW8510 compared with control group, which suggested that GW8510 increases the number of mitochondria in damaged C2C12 myotubes (Fig. 4D).

Previous studies have demonstrated that inhibition of mitochondrial fission protects against loss of muscle and impaired mitochondrial fusion interferes with oxidation of lipids in skeletal muscle (29,30), confirming that mitochondrial

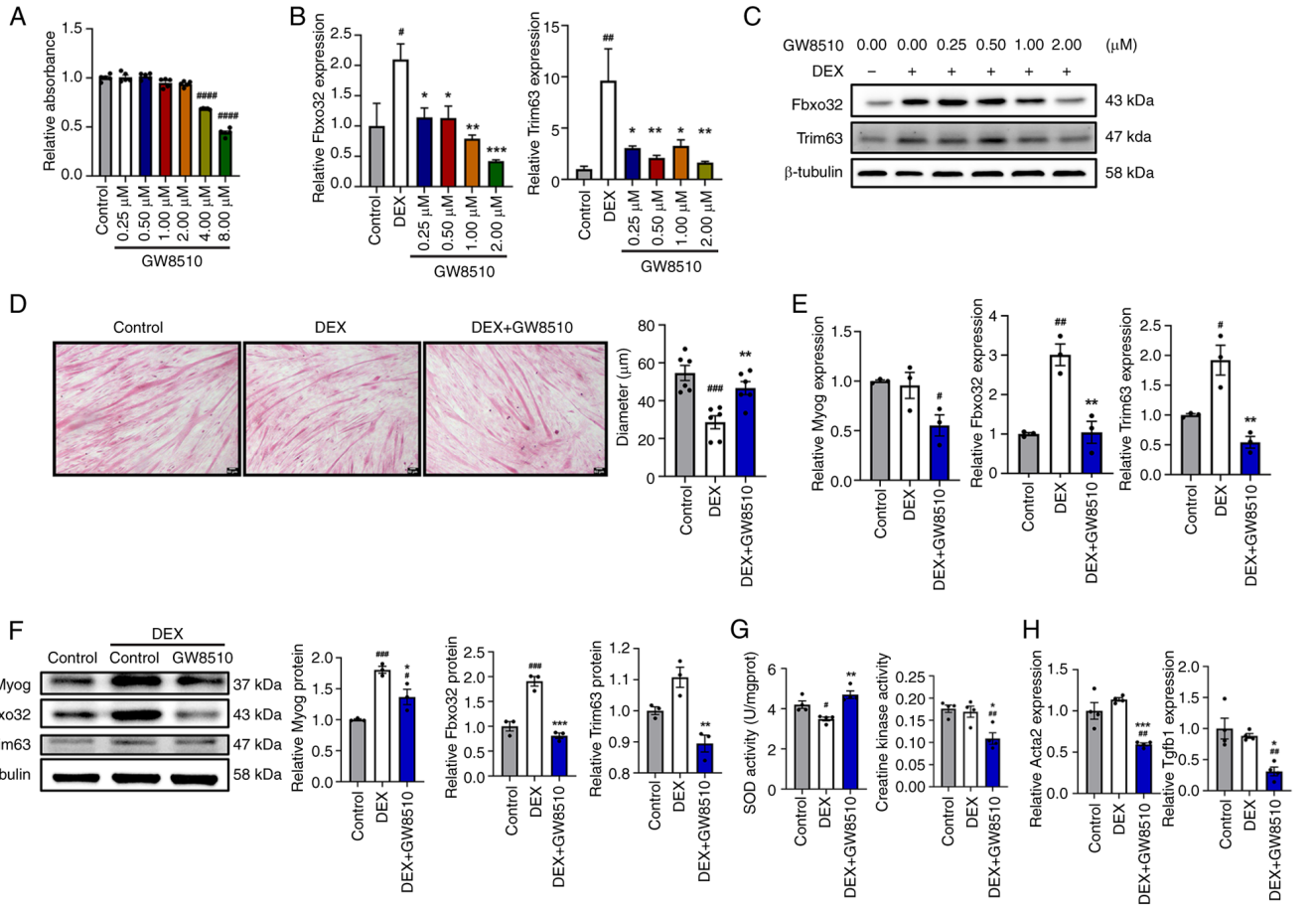

Figure 3. GW8510 ameliorates DEX-induced atrophy in C2C12 myotubes *in vitro*. (A) Viability of C2C12 myoblasts treated with GW8510 for 24 h. n=5/group. (B) Relative expression of muscle atrophy-associated genes (Fbxo32 and Trim63) in C2C12 myotubes. n=3/group. (C) Western blot analysis of muscle atrophy-associated protein (Fbxo32, and Trim63). (D) Hematoxylin and eosin staining and quantification of diameter of C2C12 myotubes. Scale bar, 50 μm. n=6/group. (E) Relative expression of muscle atrophy-associated genes (Myog, Fbxo32 and Trim63). (F) Expression levels of muscle atrophy-related protein (Myog, Fbxo32 Trim63). n=3/group. (G) SOD and creatine kinase activity. n=4/group. (H) Relative expression of muscle fibrosis-related genes (Acta2 and Tgfb) in C2C12 myotubes stimulated with DEX (10 μM) or vehicle, followed by treatment with GW8510 (2 μM) or vehicle for 24 h. n=3/group. $^{\#}$P<0.05, $^{\#\#}$P<0.01, $^{\#\#\#}$P<0.001, $^{\#\#\#\#}$P<0.0001 vs. control; *P<0.05, **P<0.01, ***P<0.001 vs. DEX. DEX, dexamethasone; Fbxo, F-box protein; Trim, tripartite motif; SOD, superoxide dismutase.

dynamics play an essential role in the development and atrophy of skeletal muscle. The present study examined the protein levels of mitochondrial fusion markers (Opa1 and Mfn1) and a mitochondrial fission marker (p-Drp1). GW8510 significantly increased the Opal protein expression and had no significant effect on the Mfn1 protein expression compared with dexamethasone group (Fig. 4E). Moreover, the p-Drp1 protein expression increased in response to stimulation with dexamethasone and decreased, albeit not to a significant extent, following treatment with GW8510 (Fig. 4E). These findings suggested that GW8510 may coordinate mitochondrial homeostasis in myotubes. The myotube has been reported to be a metabolically active cell type that is highly dependent on OXPHOS (31). Therefore, the present study examined the protein levels of OXPHOS complexes I-V. GW8510 significantly attenuated the dexamethasone-induced increase in the protein expression of complex IV but not that of complexes I, II, III and V (Fig. S6).

As Pgc1α is a key regulator of mitochondrial biogenesis (32), the present study investigated the mRNA expression of Pgc1α and other potential regulators of mitochondrial biogenesis (Tfam, Sirt1 and Nrf1) in C2C12 myotubes treated with GW8510. GW8510 significantly increased the mRNA expression of Tfam and Sirt1 and decreased the expression of Pgc1α but had no significant effect on the expression of Nrf1 compared with dexamethasone group (Fig. 4F). Overall, GW8510 improved mitochondrial function and biogenesis in C2C12 myotubes.

GW8510 increases NAD$^+$ levels and ATP production and protects against oxidative stress in vivo and in vitro. Reduced NAD$^+$ levels in aged skeletal muscle alter mitochondrial bioenergetics and have a negative effect on muscle mass, strength and endurance (33,34), indicating that low NAD$^+$ contributes to impaired mitochondrial activity and promotes progression of muscle atrophy. Therefore, the present study investigated the NAD$^+$ levels in GC tissue in denervated mice and in C2C12 myotubes. GW8510 increased the NAD$^+$ levels after treatment with GW8510 in C2C12 myotubes compared with dexamethasone group (Fig. 5A). However, the increases in the NAD$^+$ levels and the ratio of NAD$^+$ to NADH in the denervated mice were attenuated by GW8510 (Fig. 5D). Concentration of ATP decreased in both the denervated mice and in the dexamethasone-stimulated myotubes; however, the decrease

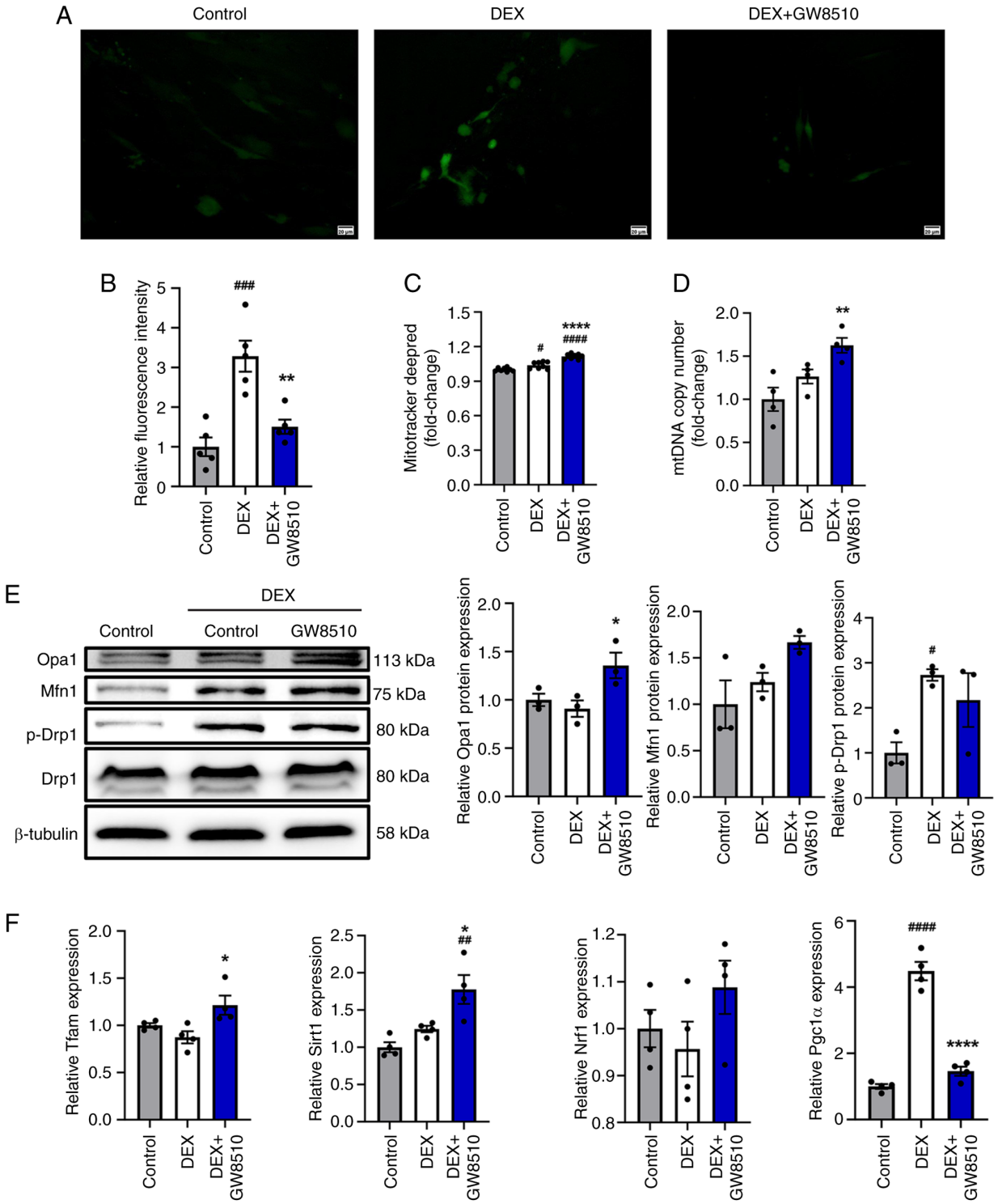

Figure 4. GW8510 improves mitochondrial function and biogenesis in C2C12 *in vitro*. (A) Reactive oxygen species staining using DCFH-DA in C2C12 myotubes stimulated with DEX (10 μM) or vehicle, followed by treatment with GW8510 (2 μM) or vehicle for 24 h. Scale bar, 20 μm. (B) Relative fluorescence intensity in C2C12 myotubes using ImageJ. n=5/group. (C) Relative mitochondrial mass using Mitotracker DeepRed staining. n=8/group. (D) Relative mtDNA copy number in C2C12 myotubes stimulated with DEX (10 μM) or vehicle, followed by treatment with GW8510 (2 μM) or vehicle for 24 h. n=4/group. (E) Western blot of mitochondrial fission and fusion-related protein (Opa1, Mfn1, Drp1 and p-Drp1). (F) Relative expression of mitochondrial biogenesis-related genes (Tfam, Sirt1, Nrf1 and Pgc1α) in C2C12 myotubes stimulated with DEX (10 μM) or vehicle, followed by treatment with GW8510 (2 μM) or vehicle for 24 h. n=3/group. $^{\#}$P<0.05, $^{\#\#}$P<0.01, $^{\#\#\#}$P<0.001, $^{\#\#\#\#}$P<0.0001 vs. control; *P<0.05, **P<0.01, ****P<0.0001 vs. DEX. DEX, dexamethasone; mtDNA, mitochondrial DNA; Mfn, mitofusin; p-Drp, phosphorylated dynamin-related protein; Tfam, transcription factor A, mitochondrial; Sirt1, sirtuin 1; Pgc, peroxisome proliferator-activated receptor gamma, coactivator.

in ATP content was significantly improved by GW8510 in C2C12 myotubes (Fig. 5B) but not in the denervated mice (Fig. 5E). Furthermore, the concentration of MDA, a marker of lipid peroxidation, increased in dexamethasone-stimulated C2C12 myotubes and GC tissue in the denervated mice, and that this increase was inhibited by GW8510 (Fig. 5C and F).

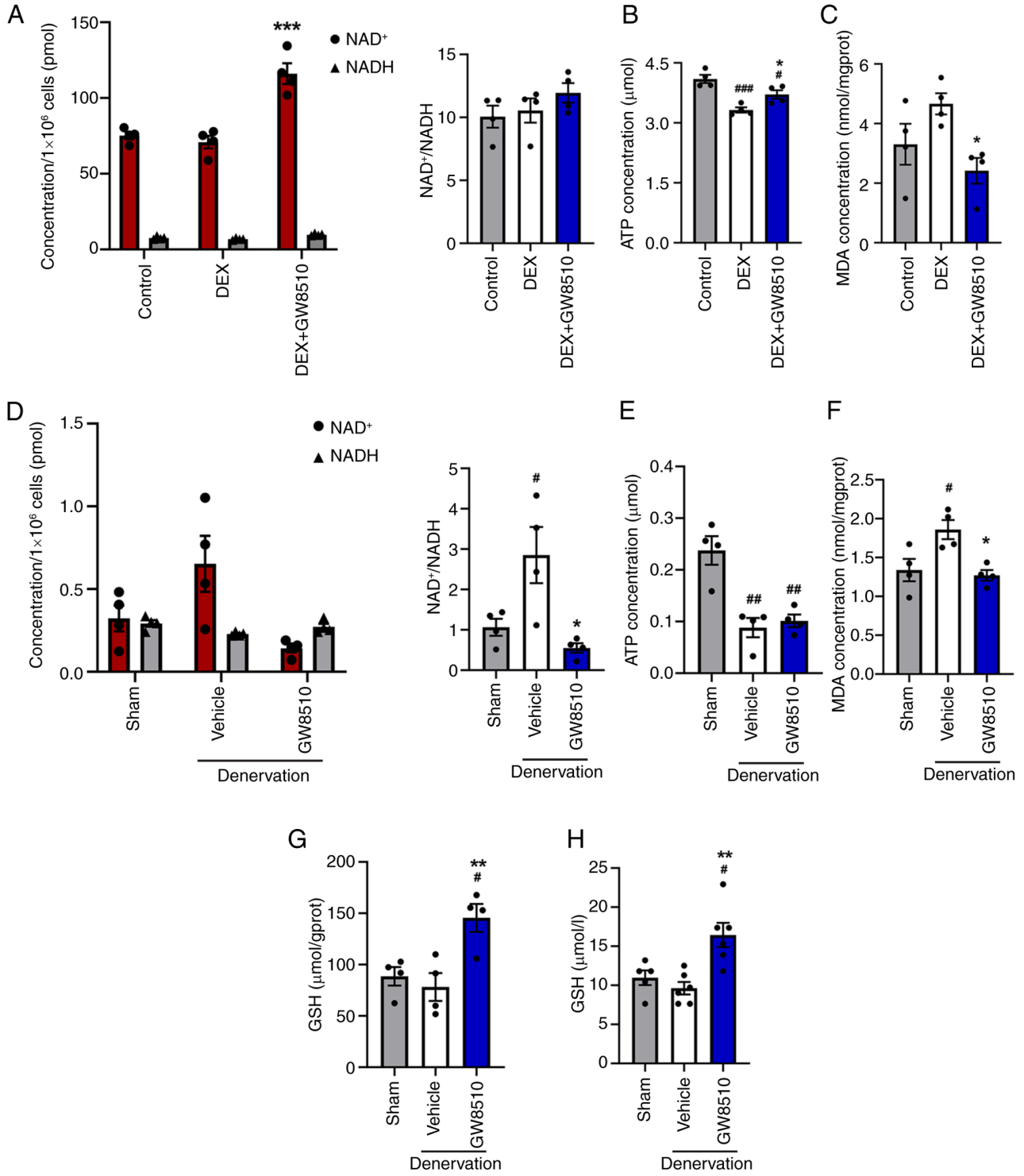

Figure 5. GW8510 increases NAD^+ levels and ATP production and protects against oxidative stress. (A) Levels of NAD^+ and NADH, and the ratio of NAD^+/NADH in C2C12 myotubes. n=4/group. Concentration of (B) ATP and (C) MDA in C2C12 myotubes stimulated with DEX (10 μM) or vehicle, followed by treatment with GW8510 (2 μM) or vehicle for 24 h. (D) Levels of NAD^+ and NADH, and the ratio of NAD^+/NADH in GC tissue. Concentration of (E) ATP and (F) MDA in GC tissue. (G). Activity of GSH in GC tissue. n=4/group. (H) Activity of GSH in serum. n=5/group. $^{\#}$P<0.05, $^{\#\#}$P<0.01, $^{\#\#\#}$P<0.001 vs. control/sham; *P<0.05, **P<0.01, ***P<0.001 vs. DEX/vehicle. MDA, malondialdehyde; DEX, dexamethasone; GC, gastrocnemius; GSH, glutathione; prot, protein.

GSH is a scavenger of free radicals, and its deficiency leads to muscle atrophy (35). Therefore, the present study examined the GSH levels in GC tissue and in the serum of denervated mice and found that the concentration in both was significantly increased by GW8510 (Fig. 5G and H). In summary, GW8510 increased NAD^+ levels and ATP production and protected against oxidative stress *in vivo* and *in vitro*.

GW8510 restores expression of genes that protect against muscle atrophy. To determine how GW8510 protects against muscle atrophy, mRNA expression in C2C12 myotubes was assessed using RNA-seq analysis. Principal component analysis identified different clusters of C2C12 myotubes in the control and in dexamethasone-stimulated mice with and without treatment by GW8510 (Fig. 6A), indicating differences

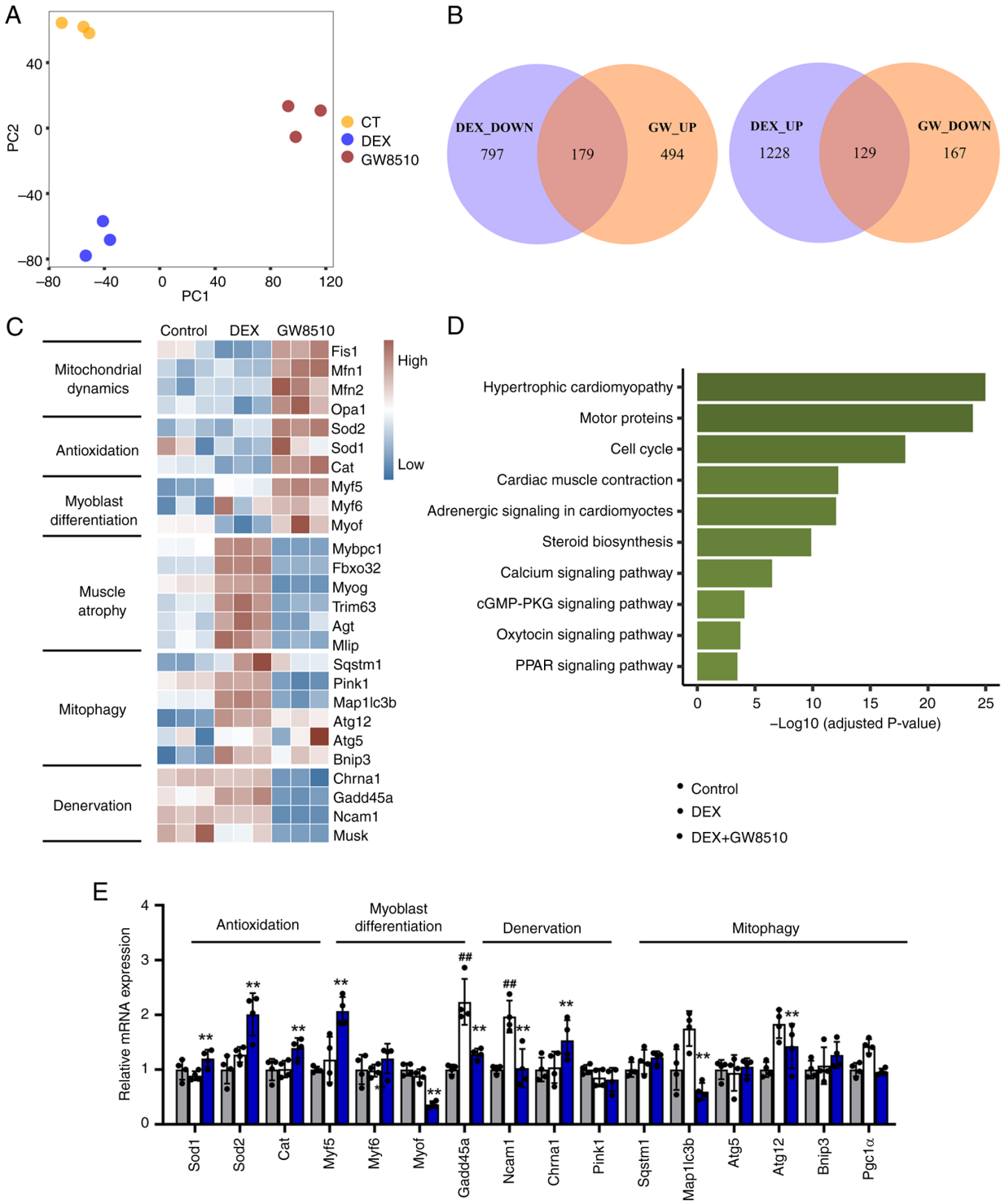

Figure 6. GW8510 exerts a protective effect on expression of genes associated with muscle atrophy and development. (A) Principal component analysis score plot on C2C12 myotubes stimulated with DEX (10 μM) or vehicle, followed by treatment with GW8510 (2 μM) or vehicle for 24 h. (B) Overlap between genes down- and upregulated by dexamethasone and GW8510. (C) Heatmap of muscle atrophy and development-associated genes, including mitochondrial dynamics- (Fis1, Mfn1, Mfn2 and Opa1), antioxidation-related genes (Sod2, Sod1 and Cat), myoblast differentiation-related genes (Myf5, MyF6 and Myof), mitophagy-related genes (Sqstm1, Pink1, Map1lc3b, Atg12, Atg5 and Bnip4) and denervation-related genes (Chrna1, Gadd45a, Ncam1 and Musk). (D) Kyoto Encyclopedia of Genes and Genomes pathway enrichment analysis for significantly differentially expressed genes. (E) Validation of relative mRNA expression of muscle atrophy- and development-associated genes. n=3/group. $^{\#\#}$P<0.01 vs. control; **P<0.01 vs. DEX. DEX, dexamethasone; PC, principal component; Fis, fission, mitochondrial 1; Mfn, mitofusin; Opa1, OPA1 mitochondrial dynamin like GTPase; Sod, superoxide dismutase; Cat, catalase; Myf, myogenic factor; Myof, myoferlin; Gadd45a, growth arrest and DNA damage inducible alpha; Ncam, neural cell adhesion molecule; Chma, cholinergic receptor nicotinic α; Pink, PTEN induced kinase; Sqstm, sequestosome; Map1lc3b, microtubule associated protein 1 light chain 3 beta; Atg, autophagy related; Bnip, BCL2 interacting protein; Pgc, peroxisome proliferator-activated receptor γ, coactivator.

in mRNA expression profiles. There were 179 overlaps between dexamethasone-induced down- and GW8510-induced upregulated genes and 129 overlaps between dexamethasone-induced up- and GW8510-induced downregulated genes

(Fig. 6B). GW8510 restored the profiles of genes associated with muscle atrophy and development, including those involved in mitochondrial dynamics [fission, mitochondrial 1, Mfn1, mitofusin 2 (Mfn2) and Opa1], antioxidation (superoxide dismutase 2 (Sod2), Sod1) and catalase (Cat)), differentiation of myoblasts (myogenic factor 5 (Myf5), Myf6) and myoferlin (Myof)], muscle atrophy [myosin binding protein C1 (Mybpc1), Fbxo32, Myog, Trim63, angiotensinogen and muscular LMNA interacting protein), mitophagy (sequestosome 1, PTEN induced kinase 1, microtubule associated protein 1 light chain 3 β (Map1lc3b), autophagy related 12 (Atg12), Atg5] and BCL2 interacting protein 3 (Bnip3)) and denervation (cholinergic receptor nicotinic α1 subunit (Chrna1), growth arrest and DNA damage inducible α (Gadd45a), neural cell adhesion molecule 1 (Ncam1) and muscle associated receptor tyrosine kinase (Musk); Fig. 6C). The 179 dexamethasone-induced down- and GW8510-induced upregulated genes were markedly enriched in muscle function and regeneration pathways, such as 'hypertrophic cardiomyopathy', 'motor proteins', 'cell cycle' and 'cardiac muscle contraction' (Fig. 6D), indicating that GW8510 exerted a protective effect on myotube differentiation. Furthermore, RNA-seq analysis confirmed that GW8510 significantly restored the expression of genes compared with dexamethasone group, including Sod1, Sod2, Cat, Myf5, Myof, Gadd45a, Ncam1, Chrna1, Map1lc3b and Atg12 (Fig. 6E). Overall, GW8510 restored expression of genes involved in muscle atrophy and development in C2C12 myotubes.

GW8510 activates the AMPK signaling cascade in C2C12 myotubes and denervated mice. Previous studies have shown that AMPK is a key regulator of muscle atrophy and mitochondrial function (36) and Mstn is a negative regulator of skeletal muscle mass; deficiency of Mstn could activate AMPK (37,38), indicating Mstn and AMPK serve an essential role in myotube differentiation. The increase in the protein expression of Mstn in dexamethasone-stimulated C2C12 myotubes was inhibited by GW8510 (Fig. 7A). GW8510 also increased the ratio of p-AMPK to AMPK in C2C12 myotubes, suggesting that GW8510 activated AMPK signaling (Fig. 7A).

To investigate the molecular mechanism of muscle atrophy, the present study examined the mRNA expression in GC and SOL tissues in the denervated mice. The mRNA levels of several atrophy-related genes (Myog, Fbxo32 and Trim63) were increased in the denervated mice and were restored to normal by GW8510 (Fig. 7B). GW8510 restored normal expression of Gadd45a and Sod1 and Sod2 (antioxidation-related genes) in GC tissue and Gadd45a and Ncam1 (denervation-related genes) in SOL tissue (Fig. S7A and B). Moreover, the protein expression of atrophy-(Myog, Fbxo32, Trim63) and mitochondrial fusion- and fission-associated genes (Opa1, Mfn1, and p-Drp1) were consistent with those expressed in C2C12 myotubes (Fig. 7C and D). GW8510 decreased the Mstn protein level and activated AMPK signaling in GC tissue in the denervated mice (Fig. 7C and D). In summary, GW8510 activated the AMPK signaling cascade in both C2C12 myotubes and mice with denervation of the sciatic nerve.

GW8510 alleviates muscle atrophy via the AMPK/PGC1α signaling cascade. A previous study showed that expression of CDK2 protein is significantly downregulated during myogenesis, indicating that CDK2 is involved in development of skeletal muscle (12). To explore the association between Cdk2 and muscle atrophy, the present study examined the mRNA and protein expression levels of Cdk2 *in vivo* and *in vitro*. The mRNA expression levels of Cdk2 decreased significantly in dexamethasone-stimulated C2C12 myotubes and GC tissue of denervated mice following treatment with GW8510 (Fig. 8A). These findings were consistent with western blot results (Fig. 8B) and indicated that inhibition of Cdk2 may serve as a potential treatment target in muscle atrophy.

Pgc1α is a key downstream target of AMPK and is associated with muscle atrophy and mitochondrial dysfunction (39-41). Therefore, the present study examined the protein expression of Pgc1α in the GC tissue in denervated mice and found that it was increased by GW8510 (Fig. 8C), indicating that GW8510 may exert a protective effect on muscle via AMPK/Pgc1α. To clarify whether this protective effect is mediated via AMPK/Pgc1α signaling, C2C12 myotubes were transfected with three siRNAs targeting Pgc1α and found that siRNA1 had the best transfection efficacy (Fig. 8D). Therefore, siRNA1 was selected for further experiments. Pgc1α is also a regulator of fatty acid oxidation and dexamethasone promotes its expression (42,43). Expression of Pgc1α was lower following transfection with siRNA targeting Pgc1α compared with negative control following dexamethasone stimulation (Fig. 8E). Protein levels of Fbxo32, Trim63, Mstn, Myog and the ratio of p-Drp1 to Drp1 in C2C12 myotubes were lower and Mfn1 in GW8510 group compared with dexamethasone group. This effect was abolished in C2C12 myotubes transfected with siRNA targeting Pgc1α (Fig. 8E), indicating that the protective effect of GW8510 was blocked when Pgc1α was knocked down.

TNFα promotes cachexia-induced muscle atrophy *in vitro* (44), indicating that TNFα could induce muscle atrophy. To avoid the effect of dexamethasone on expression of Pgc1α, siRNA targeting Pgc1α was transfected into C2C12 myotubes stimulated with TNFα with or without treatment with GW8510. Pgc1α expression was lower following transfection with siRNA targeting Pgc1α compared with siNC. Similarly, the Fbxo32, Mstn and Myog protein expression was lower and that of Mfn1 was increased in TNFα-stimulated C2C12 myotubes following treatment with GW8510 compared with siNC. This effect was abolished in C2C12 myotubes transfected with siRNA targeting Pgc1α (Fig. 8F). However, the protein level of Trim63 was not significantly different following stimulation with TNFα, indicating that there is no relationship between TNFα-induced muscle atrophy and the Trim63 levels.

Fam132b protects against atrophy of skeletal muscle in male mice via the AMPK/PGC1α pathway (45). Here, the upregulated expression levels of Fam132b and Mstn in response to stimulation with dexamethasone were attenuated by GW8510 (Fig. S7C). In the denervated mice, GW8510 also blocked ERK signaling in GC tissue and dexamethasone-stimulated C2C12 myotubes (Fig. S7D). Overall, these findings indicated that GW8510 alleviated muscle atrophy via the AMPK/PGC1α signaling cascade.

Discussion

To the best of our knowledge, the present study is the first to demonstrate that GW8510 protected against muscle loss and

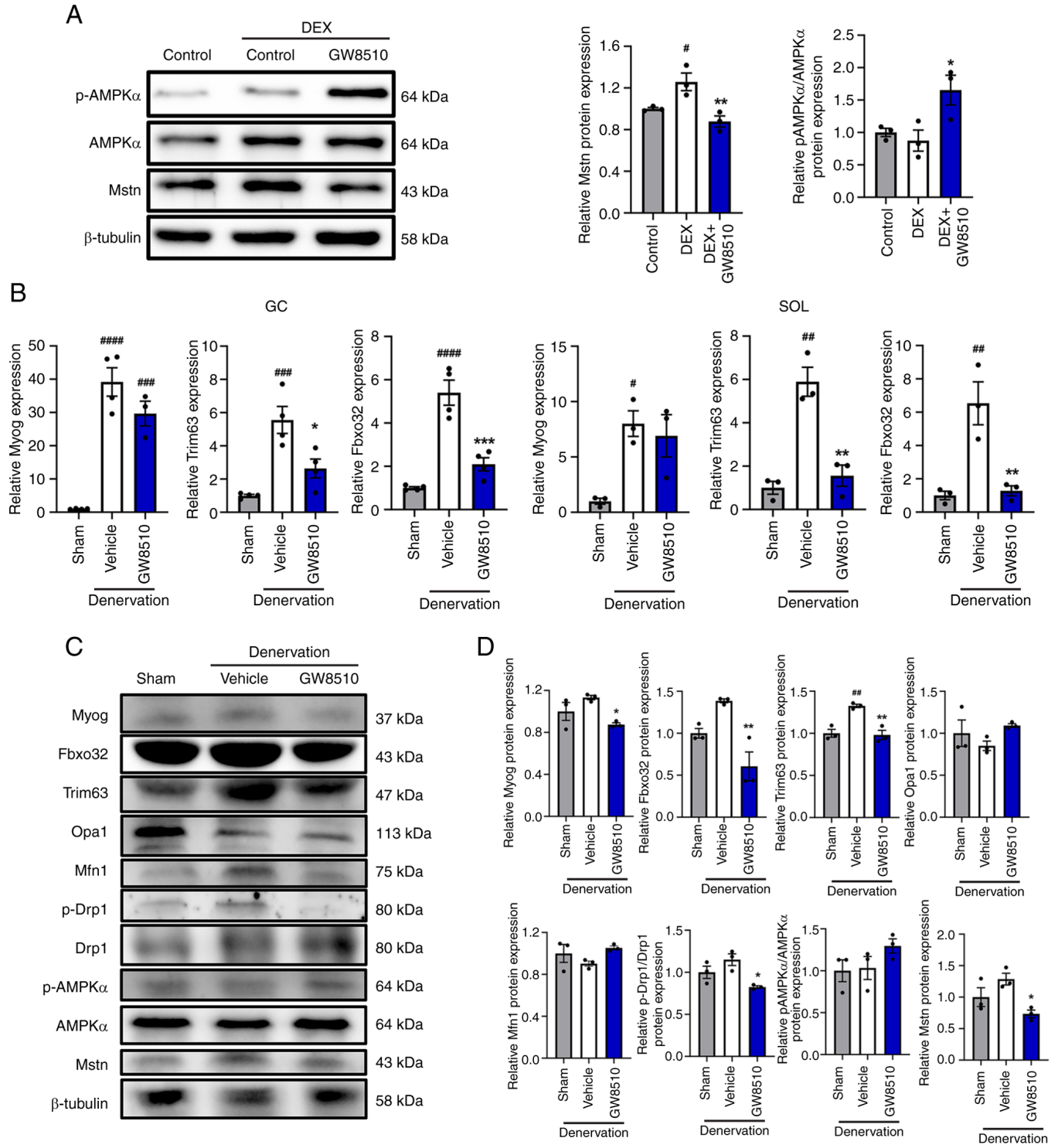

Figure 7. GW8510 activates AMPK signaling cascade in C2C12 myotubes and sciatic nerve denervation mice. (A) Western blotting of Mstn, AMPKα and p-AMPKα and quantification of relative protein levels in C2C12 myotubes stimulated with DEX (10 μM) or vehicle, followed by treatment with GW8510 (2 μM) or vehicle for 24 h. n=3/group. (B) Relative expression of muscle atrophy-related genes (Myog, Fbxo32 and Trim63) in GC and SOL tissue. n=3-4/group. (C) Western blot of muscle atrophy- (Myog, Fbxo32, Trim63) and mitochondrial fission- and fusion-related protein (Opa1, Mfn1and p-Drp1) and Mstn, AMPK, and p-AMPK in GC tissue in non-denervated, denervated and denervated mice treated with GW8510. (D) Relative protein levels. n=3/group. $^{\#}$P<0.05, $^{\#\#}$P<0.01, $^{\#\#\#}$P<0.001, $^{\#\#\#\#}$P<0.0001 vs. control/sham; *P<0.05, **P<0.01, ***P<0.001 vs. DEX/vehicle. Mstn, myostatin; p-, phosphorylated; DEX, dexamethasone; Myog, myogenin; Fbxo, F-box protein; Trim, tripartite motif; GC, gastrocnemius; SOL, soleus; Opa1, OPA1 mitochondrial dynamin like GTPase; Mfn, mitofusin; Drp, Dynamin related protein.

function. GW8510 improved the decreased weight of GC, SOL, TA, EDL and Quad and the CSA of muscle fiber, which was accompanied by enhanced muscle strength and latency to fatigue in denervation-induced muscle atrophy mice. These effects were also observed in dexamethasone- and glycerol-induced muscle atrophy mice. GW8510 enhanced the SOD activity and decreased CK activity, indicating that GW8510 improved the degree of muscle atrophy. *In vitro*, GW8510

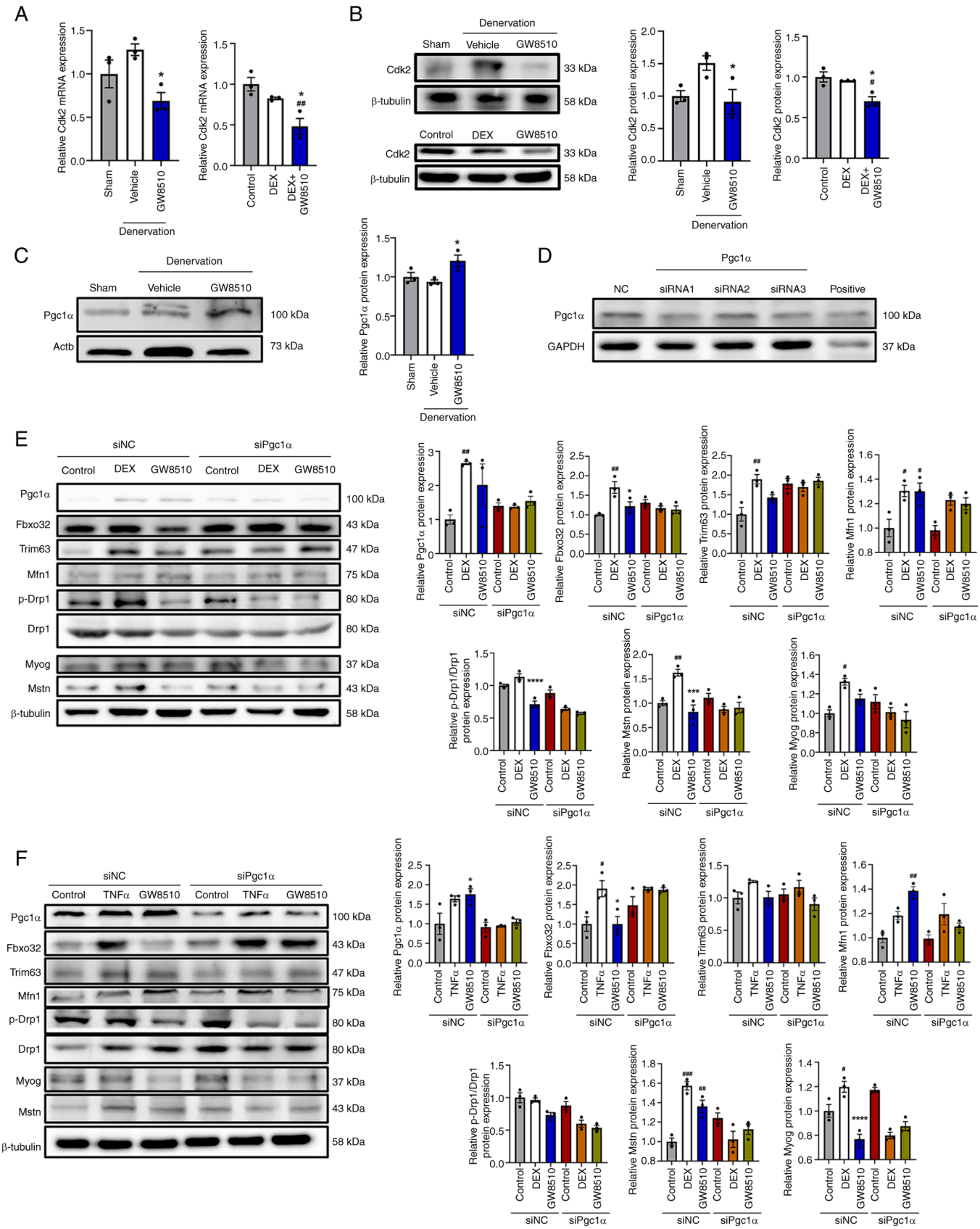

Figure 8. GW8510 alleviates muscle atrophy via the AMPK/PGC1α signaling cascade. (A) mRNA and (B) protein expression of Cdk2 in C2C12 myotubes and in GC tissue. (C). Protein expression of Pgc1α in GC tissue. (D) Western blotting of Pgc1α in C2C12 myotubes after transfection of siRNAs targeting Pgc1α. Western blotting of Pgc1α, Fbxo32, Trim63, Mfn1, Drp1, p-Drp1, Myog and Mstn in C2C12 myotubes transfected with siRNA targeting Pgc1α, followed by stimulation with (E) DEX (10 μM) or (F) TNFα (20 ng/ml) or vehicle and treatment with GW8510 (2 μM) or vehicle for 24 h. n=3/group. $^{\#}$P<0.05, $^{\#\#}$P<0.01, $^{\#\#\#}$P<0.001 vs. control/sham; *P<0.05, ***P<0.001, ****P<0.0001 vs. DEX/vehicle. PGC, peroxisome proliferator-activated receptor γ, coactivator; Cdk, cyclin dependent kinase; GC, gastrocnemius; si, Small Interfering; Fbxo, F-box protein; Trim, tripartite motif; Mfn, mitofusin; p-Drp1, phosphorylated Dynamin related protein 1; Myog, myogenin; Mstn, myostatin; DEX, dexamethasone; NC, Negative control.

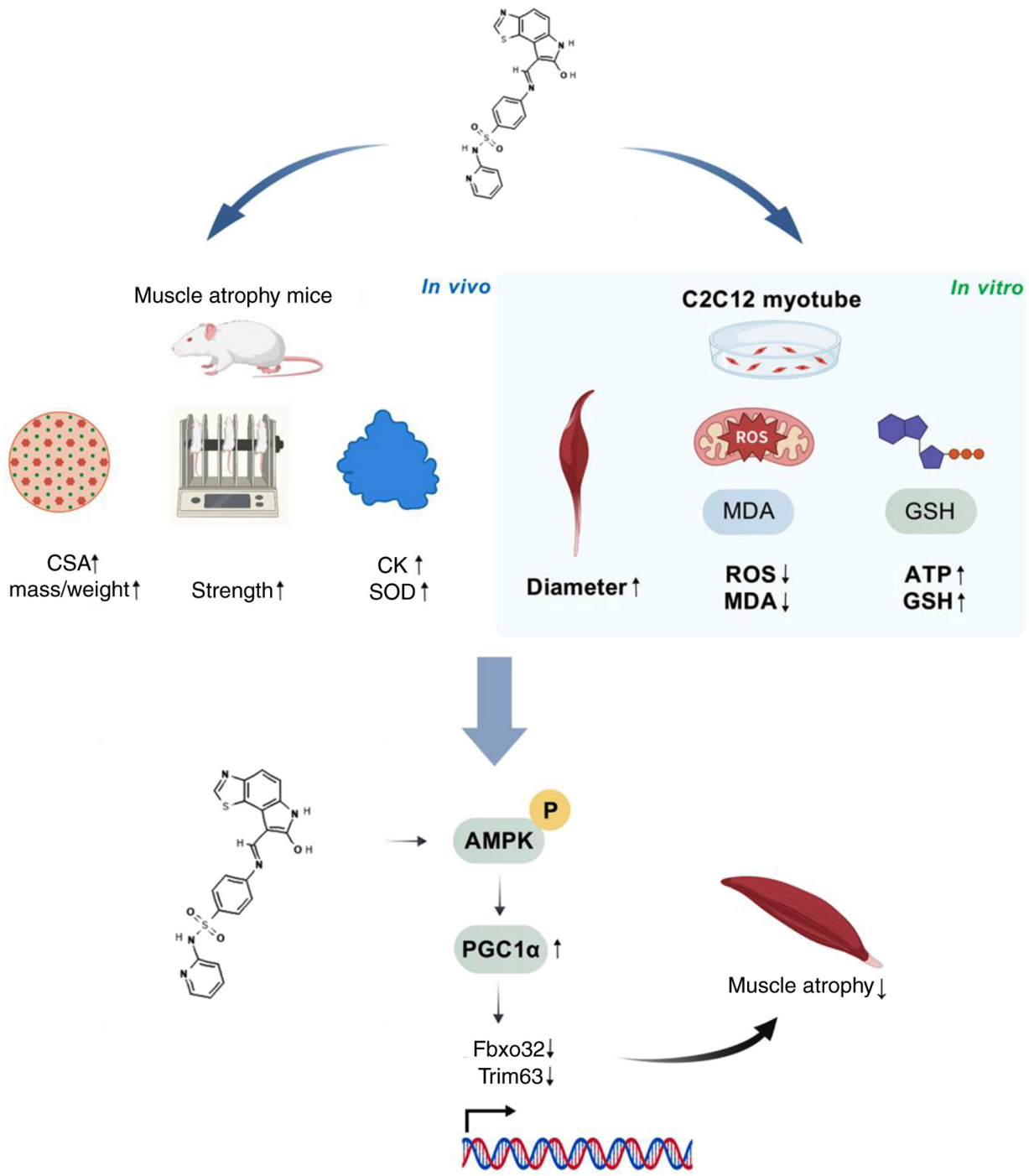

Figure 9. Proposed mechanism by which GW8510 alleviates skeletal muscle atrophy *in vitro* and *in vivo*. GW8510 inhibited muscle atrophy related-genes (Fbxo32 and Trim63) though activation of AMPK/PGC1α and decreases levels of ROS and MDA, increased the levels of ATP and GSH, thus protected against muscle atrophy. CSA, cross-sectional area; CK, creatine kinase; SOD, superoxide dismutase; ROS, reactive oxygen species; MDA, malondialdehyde; GSH, glutathione; PGC, peroxisome proliferator-activated receptor gamma, coactivator; Fbxo, F-box protein; Trim, tripartite motif. Figure created with BioGDP.com.

inhibited the mRNA and protein expression of atrophy-related genes (Fbxo32 and Trim63) and restored expression of genes associated with mitophagy, antioxidation, denervation, and myoblast differentiation. The present study demonstrated that GW8510 mediated mitochondrial function, including maintaining the homeostasis of mitochondrial fusion and fission, decreasing the production of ROS and MDA, increasing the content of NAD^+ and ATP and enhancing the GSH activity in GC tissue and C2C12 myotubes. Mechanistically, GW8510 inhibited the expression of Mstn and activated AMPK signaling. Knockdown of Pgc1α, the downstream regulator of AMPK, abolished the protective effect of GW8510. GW8510 inhibited ERK signaling in GC and C2C12 myotubes. Overall, GW8510 may serve as a novel drug to treat muscle atrophy induced by various factors and GW8510 protected against muscle atrophy via activation of AMPK/Pgc1α signaling (Fig. 9).

GW8510 is an inhibitor of CDK2/5 used to suppress the progression of various types of cancer,, such as colorectal cancer (16), pancreatic Cancer (14) and lung squamous cell carcinoma (17). CDK2 activates Rb and disrupts Myod1

function to inhibit myogenesis (12). GW8510 accelerates myotube differentiation via activation of transcription of Myod1 in human myogenic cell line LHCN-M2 (13). The present study explored the protective effect of GW8510 in muscle atrophy mouse models and mouse C2C12 myotubes. Moreover, expression of p21 is significantly induced during differentiation of skeletal muscle (46) and its expression is key for the viability of myocytes (47). Therefore, it was hypothesized that GW8510 would prevent muscle atrophy *in vitro*. In previous studies, Myog was found to activate transcription of Fbxo32 and Trim63 and be re-induced by denervation (48) (49), indicating that Myog is an upstream regulator of muscle atrophy. In this study, we found that GW8510 did not change the mRNA and protein expression of Myog compared with dexamethasone group. Overall, the downregulation of myotube atrophy-related genes following intervention with GW8510 provided more evidence to identify that GW8510 could be a potential drug to prevent the progression of muscle atrophy.

Mitochondrial dysfunction is associated with muscle atrophy. Mitochondrial degradation leads to decreased mitochondrial quality and quantity, mediated by mitophagy and the process of mitochondrial fusion and fission (50). Mitochondria are the production of site of ATP and ROS, which are involved in multiple metabolic pathways. Therefore, mitochondrial dysfunction induced by various factors, such as the disorder of ROS production and altered mtDNA copy number, contributes to muscle atrophy (51). ROS production increased in C2C12 myotubes following dexamethasone stimulation, which was decreased by GW8510, indicating that GW8510 alleviated the disorder of ROS production. Dexamethasone increased the staining of mitochondria and mtDNA copy number, indicating dexamethasone promoted mitochondrial biogenesis. GW8510 increased these indices further. Furthermore, the concentration of MDA, a marker of lipid peroxidation, increased in dexamethasone-stimulated C2C12 myotubes and GC tissue in the denervated mice, as in a previous study (52). Mitochondrial dynamics is a coordinated cycle of mitochondrial fusion mediated by Mfn1 and Opa1 and fission mediated by DRP1, which maintains the skeletal muscle and mitochondrial integrity (53). GW8510 treatment restored the protein expression of Mfn1 and Opa1 and reduced p-Drp1 levels in muscle tissue and C2C12 myotubes, although the changes were not significant., indicating the mitochondrial dynamics are complex. ATP production is dependent on OXPHOS; OXPHOS deficiency is associated with mitochondrial dysfunction (54). Here, GW8510 rescued ATP production in C2C12 myotubes with dexamethasone stimulation. Although GW8510 increased ATP levels, it did not significantly alter the protein expression of OXPHOS complex components, suggesting GW8510 may enhance ATP production by modulating ATP synthase complex regulators rather than directly affecting the protein levels of OXPHOS complex (55). NAD^+ is beneficial for preventing muscle atrophy during muscle aging (56), whereas previous studies showed that muscle NAD^+ levels increase in denervation-induced muscle atrophy in mice (57,58), suggesting that the level of NAD^+ may vary across different muscle atrophy models. Here, GW8510 increased NAD^+ levels in dexamethasone-stimulated C2C12 myotubes. GW8510 decreased NAD^+ levels in denervation-induced GC tissue, revealing that GW8510 may maintain NAD^+ levels to protect against muscle atrophy in denervation-induced mice. However, the protective effect of GW8510 on mitochondrial structure and mitophagy needs further investigation.

AMPK is a classical energy sensor that regulates various signals and metabolic pathways in response to multiple stimuli, including caloric restriction and exercise (59). It is unclear whether activation of AMPK promotes or inhibits muscle atrophy. Moreover, AMPK activity is enhanced after 4 and 7 days of denervation in mice (60,61). Metformin, an AMPK agonist, could induce muscle atrophy by activating Ampkα2 and transcriptionally regulating myostatin through HDAC6 and FoxO3a (62). However, some studies proved that myonectin, paeoniflorin and procyanidin B2 protect against muscle atrophy via AMPK signaling (41,45,63). The present study found that GW8510 increased the ratio of p-AMPK/AMPK in GC tissue and C2C12 myotubes with dexamethasone stimulation, indicating that GW8510 activated AMPK signaling. AMPK has two isoforms (Ampkα1 and Ampkα2, of which AMPKα1 is the major AMPK isoform that regulates skeletal muscle growth in mice (64). Exercise training is an effective method to prevent muscle atrophy, and studies show that exercise promotes acute AMPK activation and chronic endurance exercise training enhances AMPKα1 protein levels and activity (65-67). Moreover, activation of AMPKα1 induced by exercise requires more intensity than that required to activate AMPKα2, suggesting that activation of Ampkα1 exerts a key protective effect for maintaining muscle strength (68). Further research is required to determine whether GW8510 can activate AMPKα1 to protect against muscle atrophy.

Pgc-1α is a downstream regulator of AMPK and Sirt1 that regulates mitochondrial biogenesis and function (69,70). Furthermore, muscle-specific Pgc1α knockout mice exhibit impaired muscle function but not muscle mass (71). Moreover, Pgc1α prevents muscle atrophy by inhibiting Fbxo32 and Trim63, mediated by FoxO3 transcriptional factor (72). Here, GW8510 increased the protein expression of Pgc1α in GC tissue in denervation mice, and the protective effect of GW8510 was abolished by knockdown of Pgc1α in C2C12 myotubes following dexamethasone stimulation, indicating that GW8510 alleviated muscle atrophy via activation of AMPK/Pgc1α signaling, which may serve as a therapeutic target for muscle atrophy. Pgc1α interacts with Nrf1, a mitochondrial biogenesis-associated transcription factor, to promote the transcription of Tfam, which is key for maintaining mitochondrial DNA (73). GW8510 promoted the expression of Tfam and Sirt1 but had no significant effect on Nrf1 mRNA expression. Dexamethasone increased Pgc1α mRNA expression, potentially due to dexamethasone-induced expression of hepatic KLF9, which activated Pgc1a gene expression (42). Furthermore, a previous study demonstrated that inhibition of ERK signaling prevents muscle wasting in cachexia-induced muscle atrophy mice (74), suggesting ERK1/2 may be a therapeutic target for the treatment of muscle atrophy. Overall, ERK1/2 signaling may be a target for the prevention of muscle atrophy and requires more investigation.

Acknowledgements

Not applicable.

Funding

The present study was supported by the National Key Research and Development Program of China (grant no. 2023YFF1205103-2), National Natural Science Foundation of China (grant no. 32170756) and Beijing Life Science Academy (grant no. 2024300CD0050).

Availability of data and materials

The data generated in the present study may be found in the Gene Expression Omnibus database under accession number GSE298338 or at the following URL: https://www.ncbi.nlm.nih.gov/geo/query/acc.cgi?acc=GSE298338.

Authors' contributions

YC and ZX conceptualized the study and wrote the manuscript. YC, ZhL, MX and ZuL performed the experiments. CL and DY analyzed data. ZX edited and revised the manuscript. All authors have read and approved the final manuscript. YC and ZX confirm the authenticity of all raw data.

Ethics approval and consent to participate

All animal experiments were approved by and performed in strict accordance with the guidelines of the Ethics Committee of Peking University Health Science Centers (approval no. DLASBD0122; Beijing, China).

Patient consent for publication

Not applicable.

Competing interests

The authors declare that they have no competing interests.

References

1. Sayer AA and Cruz-Jentoft A: Sarcopenia definition, diagnosis and treatment: Consensus is growing. Age Ageing 51: afac220, 2022.
2. Petrocelli JJ, de Hart N, Lang MJ, Yee EM, Ferrara PJ, Fix DK, Chaix A, Funai K and Drummond MJ: Cellular senescence and disrupted proteostasis induced by myotube atrophy are prevented with low-dose metformin and leucine cocktail. Aging (Albany NY) 15: 1808-1832, 2023.
3. Paez HG, Pitzer CR and Alway SE: Age-Related dysfunction in proteostasis and cellular quality control in the development of sarcopenia. Cells 12: 249, 2023.
4. Bodine SC and Baehr LM: Skeletal muscle atrophy and the E3 ubiquitin ligases MuRF1 and MAFbx/atrogin-1. Am J Physiol Endocrinol Metab 307: E469-E484, 2014.
5. Cong H, Sun L, Liu C and Tien P: Inhibition of atrogin-1/MAFbx expression by adenovirus-delivered small hairpin RNAs attenuates muscle atrophy in fasting mice. Hum Gene Ther 22: 313-324, 2011.
6. Baehr LM, Furlow JD and Bodine SC: Muscle sparing in muscle RING finger 1 null mice: Response to synthetic glucocorticoids. J Physiol 589: 4759-4776, 2011.
7. Stouth DW, vanLieshout TL, Mikhail AI, Ng SY, Raziee R, Edgett BA, Vasam G, Webb EK, Gilotra KS, Markou M, *et al*: CARM1 drives mitophagy and autophagy flux during fasting-induced skeletal muscle atrophy. Autophagy 20: 1247-1269, 2024.
8. Leduc-Gaudet JP, Hussain SNA, Barreiro E and Gouspillou G: Mitochondrial dynamics and mitophagy in skeletal muscle health and aging. Int J Mol Sci 22: 8179, 2021.
9. Abrigo J, Olguín H, Tacchi F, Orozco-Aguilar J, Valero-Breton M, Soto J, Castro-Sepúlveda M, Elorza AA, Simon F and Cabello-Verrugio C: Cholic and deoxycholic acids induce mitochondrial dysfunction, impaired biogenesis and autophagic flux in skeletal muscle cells. Biol Res 56: 30, 2023.
10. Nascimento CM, Ingles M, Salvador-Pascual A, Cominetti MR, Gomez-Cabrera MC and Viña J: Sarcopenia, frailty and their prevention by exercise. Free Radic Biol Med 132: 42-49, 2019.
11. Fomina-Yadlin D, Kubicek S, Vetere A, He KH, Schreiber SL and Wagner BK: GW8510 increases insulin expression in pancreatic alpha cells through activation of p53 transcriptional activity. PLoS One 7: e28808, 2012.
12. Guo K and Walsh K: Inhibition of myogenesis by multiple cyclin-Cdk complexes. Coordinate regulation of myogenesis and cell cycle activity at the level of E2F. J Biol Chem 272: 791-797, 1997.
13. Bhanu NV, Sidoli S, Yuan ZF, Molden RC and Garcia BA: Regulation of proline-directed kinases and the trans-histone code H3K9me3/H4K20me3 during human myogenesis. J Biol Chem 294: 8296-8308, 2019.
14. Rüstem DG, Atay S, Aydin HH and Ak H: Synergistic interactions between GW8510 and gemcitabine in an in vitro model of pancreatic cancer. Anticancer Agents Med Chem 21: 2204-2215, 2021.
15. Li ZN, Shu Y, Chen CG, Li XQ, Li MY, Zhao XH, Wang S and Li J: Acquired tamoxifen resistance is surmounted by GW8510 through ribonucleotide reductase M2 downregulation-mediated autophagy induction. Biochem Biophys Res Commun 528: 554-560, 2020.
16. Hsieh YY, Chou CJ, Lo HL and Yang PM: Repositioning of a cyclin-dependent kinase inhibitor GW8510 as a ribonucleotide reductase M2 inhibitor to treat human colorectal cancer. Cell Death Discov 2: 16027, 2016.
17. Chen P, Wu JN, Shu Y, Jiang HG, Zhao XH, Qian H, Chen K, Lan T, Chen CG and Li J: Gemcitabine resistance mediated by ribonucleotide reductase M2 in lung squamous cell carcinoma is reversed by GW8510 through autophagy induction. Clin Sci (Lond) 132: 1417-1433, 2018.
18. Dong F, Guo W, Zhang L, Wu S, Teraishi F, Davis JJ and Fang B: Downregulation of XIAP and induction of apoptosis by the synthetic cyclin-dependent kinase inhibitor GW8510 in non-small cell lung cancer cells. Cancer Biol Ther 5: 165-170, 2006.
19. Johnson K, Liu L, Majdzadeh N, Chavez C, Chin PC, Morrison B, Wang L, Park J, Chugh P, Chen HM and D'Mello SR: Inhibition of neuronal apoptosis by the cyclin-dependent kinase inhibitor GW8510: Identification of 3' substituted indolones as a scaffold for the development of neuroprotective drugs. J Neurochem 93: 538-548, 2005.
20. Wimalasena NK, Le VQ, Wimalasena K, Schreiber SL and Karmacharya R: Gene expression-based screen for Parkinson's disease identifies GW8510 as a neuroprotective agent. ACS Chem Neurosci 7: 857-863, 2016.
21. Asami Y, Aizawa M, Kinoshita M, Ishikawa J and Sakuma K: Resveratrol attenuates denervation-induced muscle atrophy due to the blockade of atrogin-1 and p62 accumulation. Int J Med Sci 15: 628-637, 2018.
22. Kim HJ, Kim SW, Lee SH, Jung DW and Williams DR: Inhibiting 5-lipoxygenase prevents skeletal muscle atrophy by targeting organogenesis signalling and insulin-like growth factor-1. J Cachexia Sarcopenia Muscle 13: 3062-3077, 2022.
23. Chiu HC, Yang RS, Weng TI, Chiu CY, Lan KC and Liu SH: A ubiquitous endocrine disruptor tributyltin induces muscle wasting and retards muscle regeneration. J Cachexia Sarcopenia Muscle 14: 167-181, 2023.
24. Chen HJ, Wang CC, Chan DC, Chiu CY, Yang RS and Liu SH: Adverse effects of acrolein, a ubiquitous environmental toxicant, on muscle regeneration and mass. J Cachexia Sarcopenia Muscle 10: 165-176, 2019.
25. Livak KJ and Schmittgen TD: Analysis of relative gene expression data using real-time quantitative PCR and the 2(-Delta Delta C(T)) method. Methods 25: 402-408, 2001.
26. Mahdy MAA: Skeletal muscle fibrosis: An overview. Cell Tissue Res 375: 575-588, 2019.
27. Kubat GB, Bouhamida E, Ulger O, Turkel I, Pedriali G, Ramaccini D, Ekinci O, Ozerklig B, Atalay O, Patergnani S, *et al*: Mitochondrial dysfunction and skeletal muscle atrophy: Causes, mechanisms, and treatment strategies. Mitochondrion 72: 33-58, 2023.

28. Yokokawa T, Mori R, Suga T, Isaka T, Hayashi T and Fujita S: Muscle denervation reduces mitochondrial biogenesis and mitochondrial translation factor expression in mice. Biochem Biophys Res Commun 527: 146-152, 2020.
29. Romanello V, Guadagnin E, Gomes L, Roder I, Sandri C, Petersen Y, Milan G, Masiero E, Del Piccolo P, Foretz M, *et al*: Mitochondrial fission and remodelling contributes to muscle atrophy. EMBO J 29: 1774-1785, 2010.
30. Noone J, Rochfort KD, O'Sullivan F and O'Gorman DJ: SIRT4 is a regulator of human skeletal muscle fatty acid metabolism influencing inner and outer mitochondrial membrane-mediated fusion. Cell Signal 112: 110931, 2023.
31. Sin J, Andres AM, Taylor DJ, Weston T, Hiraumi Y, Stotland A, Kim BJ, Huang C, Doran KS and Gottlieb RA: Mitophagy is required for mitochondrial biogenesis and myogenic differentiation of C2C12 myoblasts. Autophagy 12: 369-380, 2016.
32. Yeo D, Kang C, Gomez-Cabrera MC, Vina J and Ji LL: Intensified mitophagy in skeletal muscle with aging is downregulated by PGC-1alpha overexpression in vivo. Free Radic Biol Med 130: 361-368, 2019.
33. Frederick DW, Loro E, Liu L, Davila A Jr, Chellappa K, Silverman IM, Quinn WJ III, Gosai SJ, Tichy ED, Davis JG, *et al*: Loss of NAD homeostasis leads to progressive and reversible degeneration of skeletal muscle. Cell Metab 24: 269-282, 2016.
34. Zhang H, Ryu D, Wu Y, Gariani K, Wang X, Luan P, D'Amico D, Ropelle ER, Lutolf MP, Aebersold R, *et al*: NAD^+ repletion improves mitochondrial and stem cell function and enhances life span in mice. Science 352: 1436-1443, 2016.
35. Carraro V, Combaret L, Coudy-Gandilhon C, Parry L, Averous J, Maurin AC, Jousse C, Voyard G, Fafournoux P, Papet I and Bruhat A: Activation of the eIF2α-ATF4 pathway by chronic paracetamol treatment is prevented by dietary supplementation with cysteine. Int J Mol Sci 23: 7196, 2022.
36. Kjøbsted R, Hingst JR, Fentz J, Foretz M, Sanz MN, Pehmøller C, Shum M, Marette A, Mounier R, Treebak JT, *et al*: AMPK in skeletal muscle function and metabolism. FASEB J 32: 1741-1777, 2018.
37. Shan T, Liang X, Bi P and Kuang S: Myostatin knockout drives browning of white adipose tissue through activating the AMPK-PGC1α-Fndc5 pathway in muscle. FASEB J 27: 1981-1989, 2013.
38. Rodriguez J, Vernus B, Chelh I, Cassar-Malek I, Gabillard JC, Sassi AH, Seiliez I, Picard B and Bonnieu A: Myostatin and the skeletal muscle atrophy and hypertrophy signaling pathways. Cell Mol Life Sci 71: 4361-4371, 2014.
39. Fernandez-Marcos PJ and Auwerx J: Regulation of PGC-1α, a nodal regulator of mitochondrial biogenesis. Am J Clin Nutr 93: 884s-890s, 2011.
40. Huang Y, Chen K, Ren Q, Yi L, Zhu J, Zhang Q and Mi M: Dihydromyricetin attenuates dexamethasone-induced muscle atrophy by improving mitochondrial function via the PGC-1α pathway. Cell Physiol Biochem 49: 758-779, 2018.
41. Li Q, Wu J, Huang J, Hu R, You H, Liu L, Wang D and Wei L: Paeoniflorin ameliorates skeletal muscle atrophy in chronic kidney disease via AMPK/SIRT1/PGC-1α-mediated oxidative stress and mitochondrial dysfunction. Front Pharmacol 13: 859723, 2022.
42. Cui A, Fan H, Zhang Y, Zhang Y, Niu D, Liu S, Liu Q, Ma W, Shen Z, Shen L, *et al*: Dexamethasone-induced Krüppel-like factor 9 expression promotes hepatic gluconeogenesis and hyperglycemia. J Clin Invest 129: 2266-2278, 2019.
43. Cheng CF, Ku HC and Lin H: PGC-1α as a pivotal factor in lipid and metabolic regulation. Int J Mol Sci 19: 3447, 2018.
44. Zhang HJ, Wang BH, Wang X, Huang CP, Xu SM, Wang JL, Huang TE, Xiao WL, Tian XL, Lan XQ, *et al*: Handelin alleviates cachexia- and aging-induced skeletal muscle atrophy by improving protein homeostasis and inhibiting inflammation. J Cachexia Sarcopenia Muscle 15: 173-188, 2024.
45. Ozaki Y, Ohashi K, Otaka N, Kawanishi H, Takikawa T, Fang L, Takahara K, Tatsumi M, Ishihama S, Takefuji M, *et al*: Myonectin protects against skeletal muscle dysfunction in male mice through activation of AMPK/PGC1α pathway. Nat Commun 14: 4675, 2023.
46. Parker SB, Eichele G, Zhang P, Rawls A, Sands AT, Bradley A, Olson EN, Harper JW and Elledge SJ: p53-independent expression of p21Cip1 in muscle and other terminally differentiating cells. Science 267: 1024-1027, 1995.
47. Wang J and Walsh K: Resistance to apoptosis conferred by Cdk inhibitors during myocyte differentiation. Science 273: 359-361, 1996.
48. Tang H, Macpherson P, Marvin M, Meadows E, Klein WH, Yang XJ and Goldman D: A histone deacetylase 4/myogenin positive feedback loop coordinates denervation-dependent gene induction and suppression. Mol Biol Cell 20: 1120-1131, 2009.
49. Moresi V, Williams AH, Meadows E, Flynn JM, Potthoff MJ, McAnally J, Shelton JM, Backs J, Klein WH, Richardson JA, *et al*: Myogenin and class II HDACs control neurogenic muscle atrophy by inducing E3 ubiquitin ligases. Cell 143: 35-45, 2010.
50. Sakellariou GK, Pearson T, Lightfoot AP, Nye GA, Wells N, Giakoumaki II, Vasilaki A, Griffiths RD, Jackson MJ and McArdle A: Mitochondrial ROS regulate oxidative damage and mitophagy but not age-related muscle fiber atrophy. Sci Rep 6: 33944, 2016.
51. Chen X, Ji Y, Liu R, Zhu X, Wang K, Yang X, Liu B, Gao Z, Huang Y, Shen Y, *et al*: Mitochondrial dysfunction: Roles in skeletal muscle atrophy. J Transl Med 21: 503, 2023.
52. Bellanti F, Romano AD, Lo Buglio A, Castriotta V, Guglielmi G, Greco A, Serviddio G and Vendemiale G: Oxidative stress is increased in sarcopenia and associated with cardiovascular disease risk in sarcopenic obesity. Maturitas 109: 6-12, 2018.
53. Whitley BN, Engelhart EA and Hoppins S: Mitochondrial dynamics and their potential as a therapeutic target. Mitochondrion 49: 269-283, 2019.
54. Zeviani M and Carelli V: Mitochondrial retinopathies. Int J Mol Sci 23: 210, 2021.
55. Wang T, Sun F, Li C, Nan P, Song Y, Wan X, Mo H, Wang J, Zhou Y, Guo Y, *et al*: MTA1, a novel ATP synthase complex modulator, enhances colon cancer liver metastasis by driving mitochondrial metabolism reprogramming. Adv Sci (Weinh) 10: e2300756, 2023.
56. Xu Y and Xiao W: NAD+: An old but promising therapeutic agent for skeletal muscle ageing. Ageing Res Rev 28: 102106, 2023.
57. Sonntag T, Ancel S, Karaz S, Cichosz P, Jacot G, Giner MP, Sanchez-Garcia JL, Pannérec A, Moco S, Sorrentino V, *et al*: Nicotinamide riboside kinases regulate skeletal muscle fiber-type specification and are rate-limiting for metabolic adaptations during regeneration. Front Cell Dev Biol 10: 1049653, 2022.
58. Li Y, Ma X, Li J, Yang L, Zhao X, Qi X, Zhang X, Zhou Q and Shi W: Corneal denervation causes epithelial apoptosis through inhibiting NAD+ biosynthesis. Invest Ophthalmol Vis Sci 60: 3538-3546, 2019.
59. Hsu CC, Peng D, Cai Z and Lin HK: AMPK signaling and its targeting in cancer progression and treatment. Semin Cancer Biol 85: 52-68, 2022.
60. Guo Y, Meng J, Tang Y, Wang T, Wei B, Feng R, Gong B, Wang H, Ji G and Lu Z: AMP-activated kinase α2 deficiency protects mice from denervation-induced skeletal muscle atrophy. Arch Biochem Biophys 600: 56-60, 2016.
61. Paul PK, Gupta SK, Bhatnagar S, Panguluri SK, Darnay BG, Choi Y and Kumar A: Targeted ablation of TRAF6 inhibits skeletal muscle wasting in mice. J Cell Biol 191: 1395-1411, 2010.
62. Kang MJ, Moon JW, Lee JO, Kim JH, Jung EJ, Kim SJ, Oh JY, Wu SW, Lee PR, Park SH and Kim HS: Metformin induces muscle atrophy by transcriptional regulation of myostatin via HDAC6 and FoxO3a. J Cachexia Sarcopenia Muscle 13: 605-620, 2022.
63. Xu M, Chen X, Huang Z, Chen D, Chen H, Luo Y, Zheng P, He J, Yu J and Yu B: Procyanidin B2 promotes skeletal slow-twitch myofiber gene expression through the AMPK signaling pathway in C2C12 myotubes. J Agric Food Chem 68: 1306-1314, 2020.
64. Mounier R, Lantier L, Leclerc J, Sotiropoulos A, Pende M, Daegelen D, Sakamoto K, Foretz M and Viollet B: Important role for AMPKalpha1 in limiting skeletal muscle cell hypertrophy. FASEB J 23: 2264-2273, 2009.
65. Nielsen JN, Mustard KJ, Graham DA, Yu H, MacDonald CS, Pilegaard H, Goodyear LJ, Hardie DG, Richter EA and Wojtaszewski JF: 5'-AMP-activated protein kinase activity and subunit expression in exercise-trained human skeletal muscle. J Appl Physiol (1985) 94: 631-641, 2003.
66. Campos JC, Bozi LH, Krum B, Bechara LR, Ferreira ND, Arini GS, Albuquerque RP, Traa A, Ogawa T, van der Bliek AM, *et al*: Exercise preserves physical fitness during aging through AMPK and mitochondrial dynamics. Proce Natl Acad Sci USA 120: e2204750120, 2023.
67. Wu L, Zhou M, Li T, Dong N, Yi L, Zhang Q and Mi M: GLP-1 regulates exercise endurance and skeletal muscle remodeling via GLP-1R/AMPK pathway. Biochimica et biophysica acta Mol Cell Res 1869: 119300, 2022.

68. Gibala MJ, McGee SL, Garnham AP, Howlett KF, Snow RJ and Hargreaves M: Brief intense interval exercise activates AMPK and p38 MAPK signaling and increases the expression of PGC-1alpha in human skeletal muscle. J Appl Physiol (1985) 106: 929-934, 2009.
69. Wenz T: Mitochondria and PGC-1α in aging and age-associated diseases. J Aging Res 2011: 810619, 2011.
70. Jäger S, Handschin C, St-Pierre J and Spiegelman BM: AMP-activated protein kinase (AMPK) action in skeletal muscle via direct phosphorylation of PGC-1alpha. Proc Natl Acad Sci USA 104: 12017-12022, 2007.
71. Trevino MB, Zhang X, Standley RA, Wang M, Han X, Reis FCG, Periasamy M, Yu G, Kelly DP, Goodpaster BH, *et al*: Loss of mitochondrial energetics is associated with poor recovery of muscle function but not mass following disuse atrophy. Am J Physiol Endocrinol Metab 317: E899-E910, 2019.
72. Sandri M, Lin J, Handschin C, Yang W, Arany ZP, Lecker SH, Goldberg AL and Spiegelman BM: PGC-1alpha protects skeletal muscle from atrophy by suppressing FoxO3 action and atrophy-specific gene transcription. Proc Natl Acad Sci USA 103: 16260-16265, 2006.
73. Kang D and Hamasaki N: Mitochondrial transcription factor A in the maintenance of mitochondrial DNA: Overview of its multiple roles. Ann N Y Acad Sci 1042: 101-108, 2005.
74. Penna F, Costamagna D, Fanzani A, Bonelli G, Baccino FM and Costelli P: Muscle wasting and impaired myogenesis in tumor bearing mice are prevented by ERK inhibition. PLoS One 5: e13604, 2010.